Nano Research

Open Access

Review Article

Laser-processed micro/nano electrodes for integrated devices: Architectures, mechanisms and prospects

Yihao Long[1,§], Yuanfeng Sun[2,§], Liang He[1] ✉, Ruiqi Song[1], Junyi Zheng[1], Xiaomeng Yang[6], Zhen Peng[1], Zeyu Ma[1], Wenwu Wang[1], Jibing Chen[7], Yixiao Dong[8], Shengyou Yang[9], Dan Lu[4] ✉, Hongbo Yin[5] ✉, and Peng Tian[3] ✉

[1] *School of Mechanical Engineering, State Key Laboratory of Intelligent Construction and Healthy Operation and Maintenance of Deep Underground Engineering, Sichuan University, Chengdu 610065, China*
[2] *Sleep Medicine Center, West China Hospital, Sichuan University, Chengdu 610041, China*
[3] *Institute of Optics and Electronics, Chinese Academy of Sciences, Chengdu 610209, China*
[4] *Department of Otorhinolaryngology, Head & Neck Surgery, West China Hospital, Sichuan University, Chengdu 610041, China*
[5] *Department of Ophthalmology, West China Hospital, Sichuan University, Chengdu 610041, China*
[6] *Department of Mechanical Engineering, City University of Hong Kong, Hong Kong, China*
[7] *School of Mechanical Engineering, Wuhan Polytechnic University, Wuhan 430023, China*
[8] *Pritzker School of Molecular Engineering, The University of Chicago, Chicago, IL 60637, USA*
[9] *Department of Engineering Mechanics, School of Civil Engineering, Shandong University, Jinan 250061, China*
§ *Yihao Long and Yuanfeng Sun contributed equally to this work.*

Cite this article: *Nano Research*, **2026**, *19*, 94908668. https://doi.org/10.26599/NR.2026.94908668

ABSTRACT: Ongoing miniaturization and integration of electronic devices are driving a growing demand for multifunctional and reliable micro/nano electrodes that enable microscale energy storage and harvesting. This review summarizes recent advances enabled by laser processing, an inherently maskless, precise, multi-dimensional (across one, two, and three dimensions), and designable toolkit for fabricating and enhancing micro/nano electrodes, with a focus on process–structure–property relationships, which are highly important for device and system-level implementation. Laser–material interactions are elucidated by distinguishing physical modifications from chemical transformations, and the connection between processing windows and the resulting architectures and properties is established. Laser processing plays a vital role in enhancing electrode performance, including higher specific surface area, faster ion transport, higher energy/power density, and enhanced reliability (robust cycling stability and strong substrate adhesion). Emphasis is placed on energy storage applications, including on-chip and high-energy-density micro-supercapacitors, where these miniaturized electrodes enable exceptional capacitance and electrical conductivity. Beyond energy storage, broader prospects such as multifunctional electrodes that simultaneously serve as energy storage and sensing components in compact heterointegrated devices are attracting research interest. Emerging ultrafast laser processing and combinational fabrication techniques, coupled with multifunctional hierarchical designs, are considered as effective routes toward micro/nano electrodes with higher performance and integration levels, opening avenues for next-generation integrated devices.

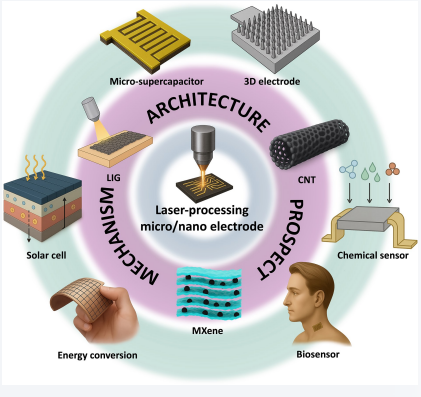

KEYWORDS: energy storage devices, micro/nano electrodes, micro-supercapacitors, laser processing, heterointegrated devices

Received: January 11, 2026; **Revised:** March 18, 2026
Accepted: March 23, 2026

✉Address correspondence to Liang He, hel20@scu.edu.cn; Peng Tian, tianpeng@ioe.ac.cn; Dan Lu, danlv2008@wchscu.cn; Hongbo Yin, hongbo_yin@163.com

1 Introduction

Currently, humanity faces common challenges in energy supply and storage as the global energy and industrial landscape accelerates toward low-carbon development. The targets of carbon peaking and carbon neutrality have catalyzed research into environmentally benign, high-performance, and reliable energy devices. To meet the

demand for localized power in heterointegrated microdevices, micro/nano electrodes have become pivotal [1]. Researchers are turning their attention to the development of more environmentally friendly, higher-performance, and more reliable energy storage devices. In addition to the traditional lithium-ion battery energy storage, emerging material families, such as graphene and other carbons, MXenes, transition-metal compounds and halides, among others, combined with structural design and interface engineering, are enabling significant achievements in energy/power density, cycle life, and environmental stability [2–5].

Translating these materials into practical devices imposes stringent manufacturing requirements for high precision, process tunability, and high-throughput scalable manufacturing. Laser processing is increasingly central to micro/nano electrode fabrication because of its high energy density, non-contact and mask-free nature, and sub-micrometer patterning resolution [6]. Representative routes include laser cutting/scribing [7], laser direct writing (LDW) and laser-induced synthesis [8], selective sintering/annealing [9], scan-irradiation activation [10], and laser-assisted three-dimensional (3D) printing. Leveraging these capabilities, next-generation micro/nano energy storage and sensing devices are being rapidly developed for wearable and flexible electronics, self-powered Internet of Things (IoT) nodes, and biomedical systems.

Recent advances in flexible electronics have increasingly shaped the development of micro/nano energy devices. Concurrently, substantial progress has been achieved in laser-enabled fabrication of energy devices tailored for flexible and deformable platforms [11, 12]. Most flexible electrodes have the form of thin films, with MXene- and graphene-based films being widely used. In addition, due to the rapid growth of flexible and wearable electronics, an urgent demand for energy devices with higher energy density and fast charging capabilities to sustain long-term operation is raised [13–16]. Laser processing also plays a vital role in tailoring electrode properties or achieving new functionalities, such as processing antibacterial biofilm electrodes [17] and silver electrodes [18] with remarkable adhesion strength. These emerging energy devices are being deployed across a broad range of technologies, with particularly rapid advances in next-generation sensors [19–21]. In the future, the development of ultrafast lasers will lead to new and broad development prospects for the manufacture of energy devices.

Accordingly, this review focuses on laser-enabled materials and manufacturing strategies for multifunctional, highly reliable micro/nano electrodes and their roles in energy storage, supply, and conversion, as shown in Fig. 1. We first delineate laser–material interactions, including separating physical mechanisms (ablation, texturing, and sintering) from chemical transformations (reduction, doping, and phase change), and link processing windows to structural dimensions (one-dimensional (1D), two-dimensional (2D), and 3D) and electrochemical performance/reliability. Laser-based fabrication strategies for micro/nano electrodes are then elaborated, with advances related to dimensional architecture discussed and evaluated in micro-supercapacitors (MSCs), sensors,

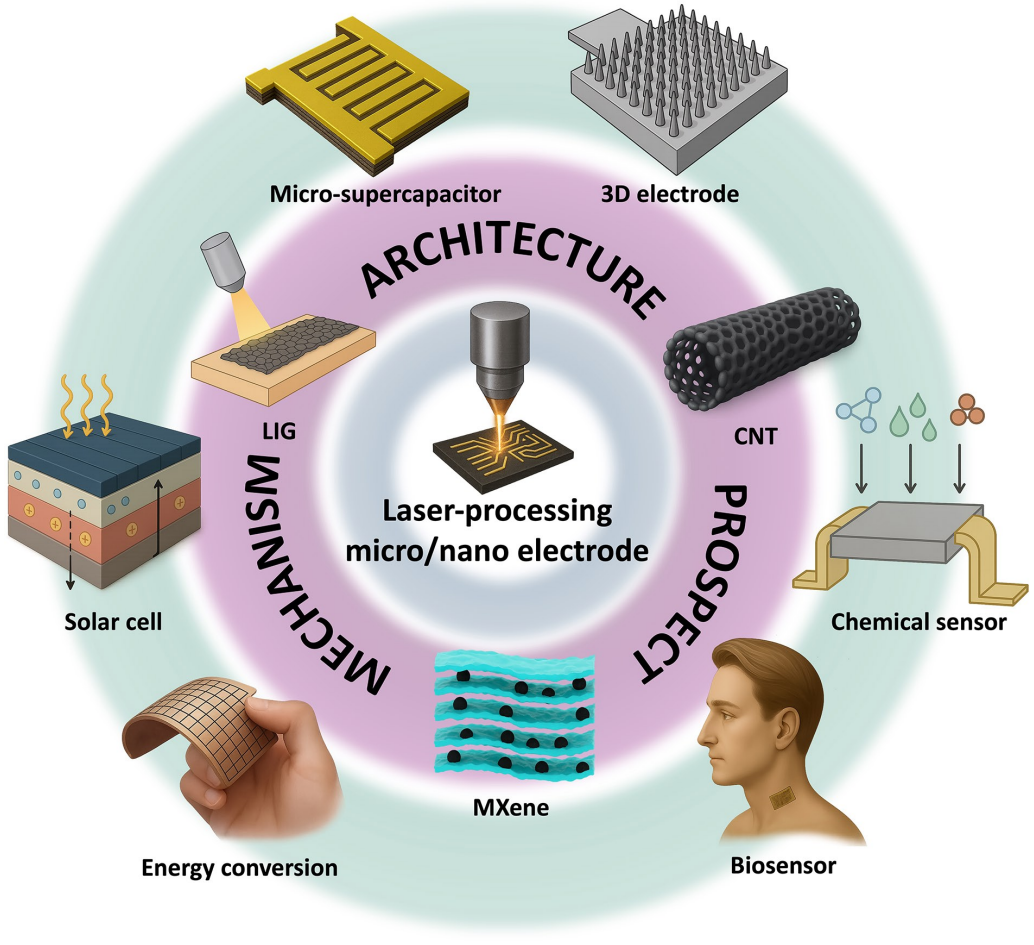

Figure 1 Laser-processed micro/nano electrodes for highly integrated devices.

and transducers. Finally, we highlight current challenges, including scalability and uniformity, back-end-of-line (BEOL) compatibility, and long-term stability, while outlining opportunities in ultrafast laser routes, data-guided design, and co-integration with energy harvesters that will shape the next generation of heterointegrated energy storage and sensing devices.

2 Laser processing techniques of micro/nano electrodes

2.1 Laser–material interactions

Laser processing is an ideal technique for fabricating micro- and nanoscale electrodes because it is a non-contact method that interacts with the material without requiring a physical tool. This avoids tool wear or contamination and allows easy working on delicate or complex architectures [22–24]. Also, lasers offer exceptional precision and control, allowing the regulated beam to be tightly focused to a small spot, enabling patterns with micrometer or nanometer features [25]. This means highly localized processing: the laser induces changes only in the targeted area without affecting non-irradiated regions. As a result, one can modify a material's surface or structure in a very confined zone, which is crucial for making tiny electrodes without collateral damage to nearby structures. Moreover, laser parameters are easily tunable (energy, focus, scanning path), providing fine control over the fabrication process. Unlike traditional photolithography, LDW requires no masks, providing great flexibility in design and the ability to pattern arbitrary shapes in real time. It is also a high-efficiency, rapid process, as laser fabrication can often be completed in a short time while achieving high-quality results. For micro/nano electrodes that demand precision and minimal damage to the substrate, laser processing offers a precise, controllable, and clean approach that is well-suited to the task.

Building upon the aforementioned summary, we define laser processing for micro/nano electrode fabrication as the dominant outcome at the interaction zone. Processes that primarily use a laser to ablate or remove the sacrificial layer are classified as physical pathways. Examples include several bottom-up processes, such as sintering or deposition, and top-down approaches, such as ablation, etching, cutting, or scribing, as well as welding methods, all of which involve negligible volume change. As for the laser-processing driving covalent bond cleavage/formation, it can be defined as chemical pathways, including photothermal/photochemical reduction, laser annealing/doping, and irradiation-enabled surface chemistry. The subsequent subsections follow this taxonomy and correlate process windows with structural, compositional, and performance metrics.

2.2 Physical modification

Laser processing enables localized, maskless, and programmable modification of materials for micro/nano manufacturing, including additive, subtractive, and joining operations. This enables structural shaping and fine patterning of energy device components. Physical modification methods by laser processing are generally categorized as bottom-up (constructing structures by additive assembly or consolidation) or top-down (removing or etching substances to create structures) techniques, depending on how the material's volume is changed during processing. Herein, we summarize representative processing routes and application examples, while the underlying multiphysics mechanisms and their dimension-dependent orchestration are discussed in Section 3.4.

2.2.1 *Bottom-up approaches*

Bottom-up laser processing includes techniques such as laser sintering and laser deposition. In laser sintering, often used in additive manufacturing, a powder layer is deposited and then selectively fused by a laser according to a designed pattern, which melts the powder in specific regions, and upon solidification, a solid layer of the desired structure is formed. By repeating this process layer by layer, a 3D structure can be built. However, the processing efficiency of layerwise laser sintering is relatively low, as each layer has to be processed individually [26]. Many researchers have systematically investigated laser sintering technology and its applications in manufacturing, highlighting its versatility for fabricating complex parts (including porous electrodes and solid electrolytes) with fine control [27, 28]. Laser-based directed energy deposition (LDED) feeds material (typically metal powder or wire) into a laser-generated melt pool to assemble structures layer-by-layer. LDED is particularly suitable for fabricating functionally graded metals with spatially tailored compositions and properties [26, 29].

Recent advances demonstrate the growing potential of laser sintering for energy storage device fabrication. For instance, Zhang et al. [26] reported the one-step laser sintering of an Al/Ni powder mixture to create compact Li-ion battery (LIB) anodes without any binder or separate current collector, as shown in Fig. 2(a). By adjusting the ratio of Al/Ni and laser parameters, they obtained a porous alloy anode containing multiple intermetallic phases (Al, Al_3Ni_2, Al_3Ni, and Ni) that formed a robust conductive network. The laser-sintered electrode exhibited a high capacity (522.8 $mAh \cdot g^{-1}$ after 200 cycles) and excellent rate performance, retaining 338.4 $mAh \cdot g^{-1}$ at 2 $A \cdot g^{-1}$. In another example, Ramos et al. [30] developed an ultrarapid CO_2-laser sintering technique to densify garnet-type solid electrolytes for solid-state batteries, as shown in Fig. 2(d). Their laser process could sinter a Li-garnet electrolyte film to high density within seconds, yielding a thin, crack-free ceramic layer that overcomes the processing difficulties of conventional furnace sintering.

2.2.2 *Top-down approaches*

Top-down laser processing refers to subtractive or structuring techniques such as laser etching, cutting, drilling, and scribing. In these methods, a focused laser beam locally removes material (by ablation), thereby removing portions of a substrate to form the desired pattern or micro/nano structure. Because laser ablation is a maskless, direct-write process, it can rapidly produce fine features without the need for complex lithography. This makes it attractive for miniaturizing energy devices (e.g., patterning micro-electrodes or flow channels in batteries, supercapacitors, and fuel cells). Recent studies have leveraged laser ablation to obtain fine-patterned micro/nano electrodes.

For instance, Huang et al. [31] achieved high-performance planar MSCs by laser-ablating MXene films into interdigital electrode patterns, as shown in Fig. 2(b). Precise laser patterning, combined with an optimized ink formulation to prevent nanosheet restacking, produced uniform microelectrodes that delivered an ultrahigh volumetric energy density of about 75 $mWh \cdot cm^{-3}$ at an operating voltage of 1.2 V. In another study, Chen et al. [32] developed a laser-assisted paste-tear technique to fabricate flexible

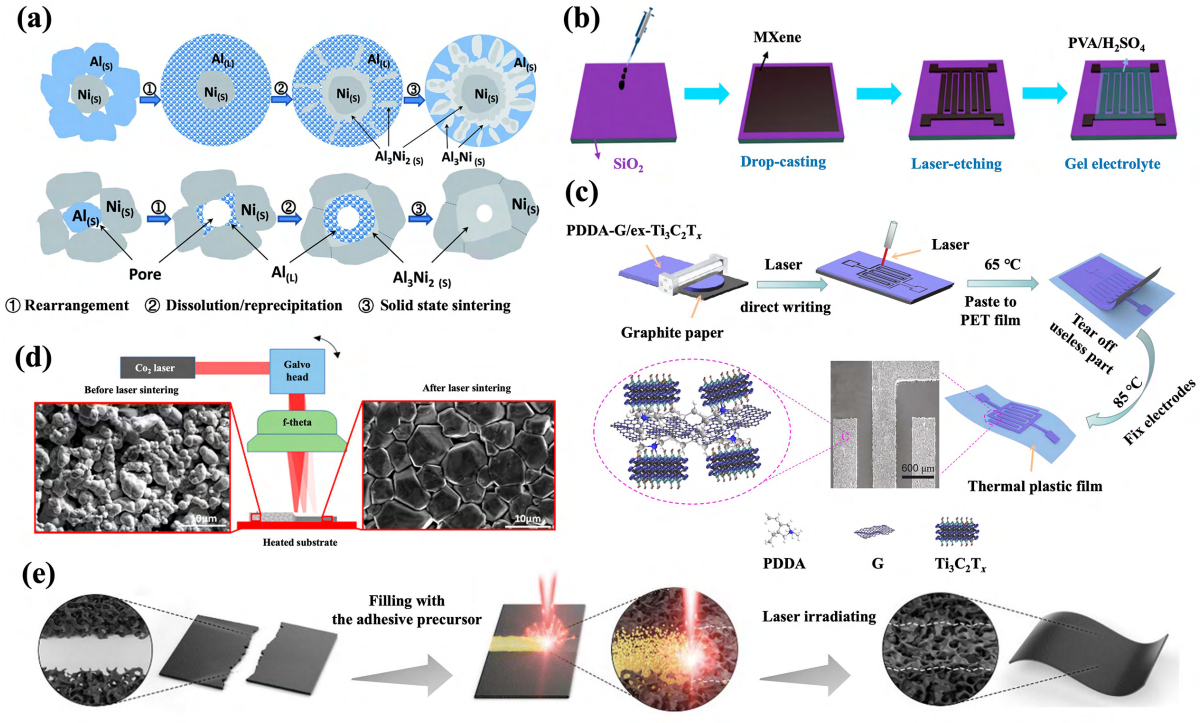

Figure 2 (a) Schematic diagram of the microstructure evolution of the Al/Ni integrated electrodes. Reproduced with permission from Ref. [26], © The Royal Society of Chemistry 2022. (b) Schematic illustrating the fabrication process of MXene-based on-chip MSC. Reproduced with permission from Ref. [31], © American Chemical Society 2022. (c) Schematic diagram of the manufacturing process for poly(diallyldimethylammonium chloride) (PDDA) functional reduced graphene oxide/exfoliate $Ti_3C_2T_x$ (PDDA-G/ex-$Ti_3C_2T_x$) symmetrical MSC. Reproduced with permission from Ref. [32], © Elsevier B.V. 2022. (d) Schematic illustration of CO_2 laser sintering of the $Li_{6.4}La_3Zr_{1.4}Ta_{0.6}O_{12}$ green films. Reproduced with permission from Ref. [30], © American Chemical Society 2022. (e) Schematic illustration of the PLW process for porous graphene film. Reproduced with permission from Ref. [33], © The Royal Society of Chemistry 2023.

MXene MSC arrays on polymer substrates, as shown in Fig. 2(c). In this method, an MXene composite film was coated on polyethylene terephthalate (PET) and then cut into a kirigami-inspired pattern by laser, after which the selected regions were peeled to produce a modular array of interdigital MSCs. The resulting MSC exhibited a high areal capacitance (241 mF·cm^{-2}) and maintained robust mechanical stability under repeated bending, stretching, and twisting. Overall, laser etching and cutting enable scalable fabrication of MSC with a precise pattern control and preserved electrical/mechanical performance.

Laser structuring has also been applied to thick battery electrodes to achieve improved high-rate performance and cycling durability [34]. For instance, laser-patterning a thick $Li(Ni_{0.6}Mn_{0.2}Co_{0.2})O_2$ (NMC622) cathode increased its capacity by up to 60 mA·h·g^{-1} at high current densities, while cutting the cell's ionic resistance by about 65%. Over long-term cycling, the structured electrodes retained ~ 30% more capacity after 500 cycles compared with unstructured electrodes, demonstrating improved durability.

In addition to material removal, laser processing can be used in a top-down manner to join or fuse materials with minimal bulk melting, which is a process known as laser welding. For example, ultrafast laser pulses have been employed to weld the junctions in silver nanowire (AgNW) networks, transforming a percolating nanowire film into a more continuous, robust transparent conductor. Laser nanowelding of AgNWs markedly decreases the sheet resistance of the film (down to 14.7 Ω·sq^{-1} at a transmittance of 89.5%) without damaging the flexible substrate [35]. The welded AgNW network also exhibits excellent mechanical durability, maintaining stable electrical conductivity even after 10,000 bending cycles. Chen et al. [36] demonstrated that using a low-power laser to sinter the contacts between AgNWs significantly improved the integrity of the nanowire networks, yielding a transparent conductive film with high electromagnetic interference (EMI) shielding effectiveness, yet maintaining light transmittance over 85%. This approach shows promise for replacing traditional indium tin oxide in flexible electronics and displays. Likewise, graphene films and architectures can be bonded by laser welding.

Yu et al. [33] reported a pulsed laser welding (PLW) strategy to directly join macroscopic 3D graphene frameworks, which is normally challenging because graphene cannot be easily melted or soldered by conventional methods, see in Fig. 2(e). In their approach, a specially designed carbon precursor was converted into a graphene solder by laser irradiation, enabling strong junctions between separate porous graphene pieces. The resulting welds showed high electrical conductivity (6700 S·m^{-1}) and tensile strength (7.3 MPa), comparable or superior to the graphene framework itself. The dimension-dependent mechanism–property relationships of laser welding (e.g., junction resistance reduction and fatigue reliability) are discussed in Section 3.4.1.

2.3 Chemical transformations

Laser-enabled chemical transformations provide a maskless route to tailor electrode chemistry and microstructure. In general, these transformations can be categorized into: photoreduction/deoxygenation of oxide precursors, laser-induced carbonization/graphitization of polymeric or organic precursors, and post-treatments such as laser annealing/activation and functionalization to tune defect density and surface chemistry. This section

summarizes representative transformation routes and outcomes, while their dimension-dependent orchestration with processing steps is discussed in Section 3.4.

2.3.1 *Laser reduction*

Among chemical transformations, laser-driven deoxygenation of graphene oxide (GO) is a widely used route to obtain conductive reduced graphene oxide (rGO)/graphene with tunable porosity or micro-energy-storage electrodes. Laser irradiation can drive rapid deoxygenation of GO, simultaneously improving electrical conductivity and inducing porous structures beneficial for electrolyte access. A typical example, reported by Gao et al. [37], as shown in Figs. 3(a) and 3(b), is the fabrication of MSCs by direct laser etching on hydrated GO films, yielding MSCs with a specific capacitance of 0.51 mF·cm^{-2} (in-plane geometry), a volumetric capacitance of 3.1 F·cm^{-3}, and an energy density of 4.3 × 10^{-4} Wh·cm^{-3}. The MSCs also showed a high cycling stability, retaining 65%–70% of their initial capacitance after 10,000 cycles. Lee et al. [38] obtained multilayer graphene by laser reduction of Zn-infiltrated GO (Fig. 3(c)). They demonstrated that simple pre-treatment of GO can markedly enhance the electrochemical performance of the resulting graphene. The graphene obtained by reducing zinc-impregnated GO showed higher performance than that obtained by direct laser reduction of GO (LrGO): The specific surface area increased from 277 to 378 m^2·g^{-1}, and the pore volume increased from 0.91 to 1.72 cm^3·g^{-1}. Fu et al. [40] fabricated porous composites by laser reduction of nitrogen-rich carbon nanoparticles and GO composites (NCNPs@GO). They also demonstrated that the reduced NCNPs@GO composite supercapacitors exhibit relatively higher specific capacitance and higher rate performance than naked rGO-based supercapacitors prepared by the same method.

2.3.2 *Laser-induced graphene*

To avoid the need for GO precursor preparation, laser-induced graphene (LIG) enables direct conversion of carbon-rich precursors into porous graphene-like networks. Lin et al. [4] developed a facile and scalable method to directly obtain 3D porous graphene by laser irradiation on the surface of a carbon-based precursor such as polyimide (PI), as shown in Fig. 3(d). They subsequently outlined two pathways for large-scale manufacturing: a roll-to-roll method for in-plane electronics and 3D-printed LIG at the macro scale. They further claimed LIG's various applications, from renewable energy equipment to water treatment platforms. Comprehensive reviews have summarized LIG preparation and functionalization for sensing applications [41, 42]. Herein we emphasize LIG by a scalable laser-induced carbonization route that yields porous, conductive networks suitable for integrated micro devices.

Laser scribing is another method for producing graphene. A typical example is the synthesis of grass laser-scribed graphene (LSG) on ordinary polyimide plastic via direct laser induction, reported by Xu et al. [39] (Fig. 3(e)). It is used as a disposable electrochemical sensor for the detection of three neurotransmitters, dopamine (DA), epinephrine (EP), and norepinephrine (NE). Fenzl et al. [43] fabricated LSG electrodes on polyimide foils using a direct write laser process, and prepared highly sensitive and reliable biosensors for serum analysis. Alhajii et al. [44] fabricated LSG interlayers to inhibit polysulfide shuttle in Li-S batteries.

2.3.3 *Laser irradiation*

Beyond precursor conversion, laser irradiation can serve as a versatile post-treatment to tailor near-surface chemistry, defect configurations, and microstructure without inducing bulk melting, particularly under ultrafast irradiation [45, 46]. Compared with conventional thermal annealing, laser post-treatments offer

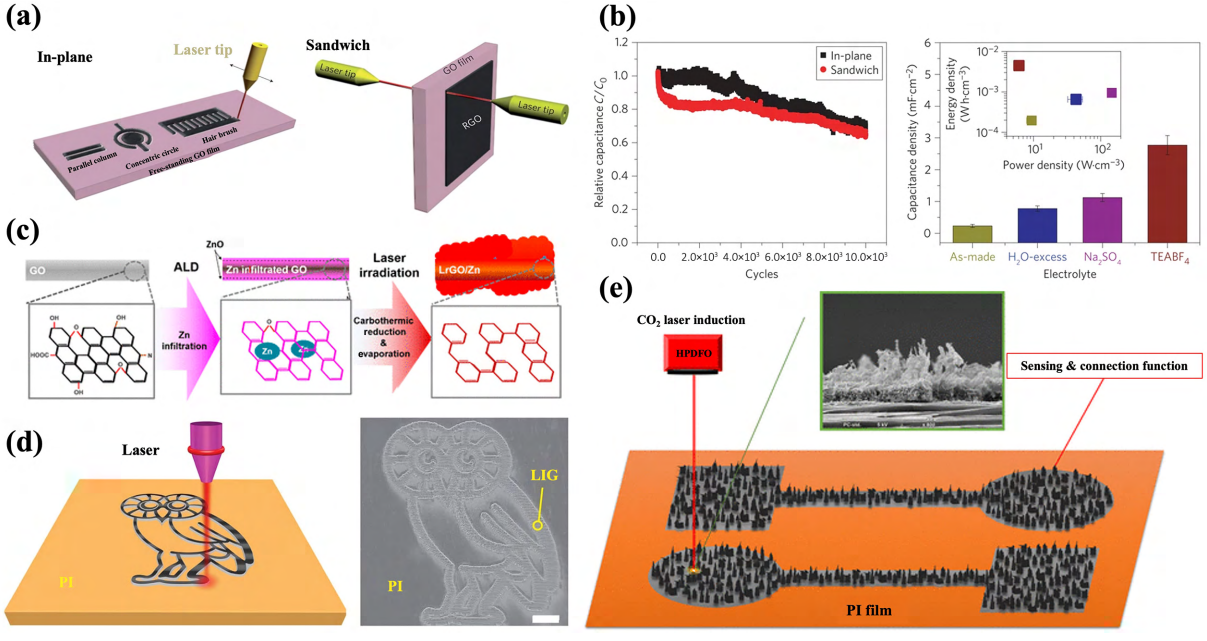

Figure 3 (a) Schematics of CO_2 laser-patterning of free-standing hydrated GO films to fabricate RGO–GO–RGO devices with in-plane and sandwich geometries. Reproduced with permission from Ref. [37], © Springer Nature Limited 2011. (b) Long-term cyclability of sandwich and concentric circular devices. Reproduced with permission from Ref. [37], © Springer Nature Limited 2011. (c) Schematic showing the synthesis route of the multilayered graphene using laser reduction. Reproduced with permission from Ref. [38], © American Chemical Society 2019. (d) Schematic of the synthesis process of LIG from PI. Reproduced with permission from Ref. [4], © Lin, J. et al. 2014. (e) Schematic representation of LSG grass fabricated by CO_2 laser induction. Inset: the cross-sectional SEM view of LSG grass. Reproduced with permission from Ref. [39], © American Chemical Society 2018.

localized, maskless, and spatially programmable modification, enabling on-demand tuning of electrode interfaces after patterning/structuring [52]. In practice, such treatments can increase structural ordering and electrical conductivity via localized annealing/defect healing, which has been widely reported in carbonaceous systems [53], regulate surface energy and wettability to promote electrolyte wetting/penetration and reduce interfacial impedance, an effect that has been highlighted as a key benefit of laser-structured electrodes at the cell level [54]. The treatments also introduce, rearrange, or stabilize surface functional groups and heteroatom configurations (e.g., N/S/O), thereby creating additional redox-active sites and improving charge-transfer kinetics [55]. These outcomes can be achieved through low-power raster scanning, multi-pass irradiation, and/or atmosphere-assisted processing (e.g., inert/reducing or heteroatom-containing environments), which allows controllable surface activation/doping while preserving the electrode architecture. As a result, laser post-treatments are often employed as finishing steps after structuring/patterning to ensure clean, stable, and well-wetted interfaces for subsequent electrolyte infiltration and device packaging. Representative examples of laser-fabricated micro/nano electrodes produced via different processing routes are summarized in Table 1.

3 Micro/nano electrodes by laser-processing

Across micro/nano electrodes, structure and materials modification co-evolve under three coupled constraints, consisting of transport, mechanics, and integration [6, 56]. Effective designs shorten ion pathways and ensure continuous electron percolation while

Table 1 Comparison of laser-fabricated micro/nano electrodes across processing routes

Processing route	Laser regime/key parameter knobs	Material/substrate	Fabricated structure	Performance metrics	Ref.
Laser sintering	One-step laser sintering	Al/Ni powder mixture	Porous alloy anode with intermetallic phases (Al, Al_3Ni_2, Al_3Ni, and Ni)	522.8 mAh·g^{-1} after 200 cycles; 338.4 mAh·g^{-1} at 2 A·g^{-1}	[26]
Laser sintering	CO_2 laser scanning + heating stage	Garnet-type solid electrolyte	Rapid densification of electrolyte layer; thin, dense, and crack-free ceramic	High relative density of 95.68%; high conductivity of 0.26 mS·cm^{-1} at 25 °C; low activation energy of 0.38 eV	[30]
Laser sintering	Infrared laser sintering (post-processing)	3D printed Al nanoparticle anode (Al–air battery)	Printed Al anode; laser sintering improves particle contacts and removes solvent	Discharge capacity of 239 mAh·g^{-1} and an operation voltage of 0.95 V	[47]
Laser ablation	Patterned region of 6 mm × 6 mm	$Ti_3C_2T_x$ MXene film on Si/SiO_2 wafer	Interdigital electrodes: finger width ~ 480 μm, gap ~ 74 μm; MXene film thickness of 1.13 μm (W/A = 0.5)	Areal capacitance of 39.6 mF·cm^{-2} at 10 mV·s^{-1}; volumetric capacitance of 350.4 F·cm^{-3}; volumetric energy density of 75.5 mWh·cm^{-3} at 1088 mW·cm^{-3} with an ultrahigh operating voltage of 1.2 V; capacitance retention of 85.5% after 12, 000 cycles	[31]
Laser ablation	Laser ablation structuring; knobs include laser power/scan strategy	Thick NMC622 cathodes (aqueous processed)	Laser-generated 3D grooves/channels in thick cathodes	Capacity increases up to 60 mAh·g^{-1} at high rate; 65% decrease in ionic resistance; 29%–38% higher capacity after 500 cycles	[48]
Laser cut	Pulse width of 10 μs; speed of 100 mm·s^{-1}; frequency 25 Hz	MXene composite film on PET	8-finger interdigital MSC: finger width of 456 μm, finger length of 5 mm, gap of 333 μm; active layer thickness of 43 μm (graphite paper: 140 μm)	Areal capacitance of 241 mF·cm^{-2}; areal energy density of 12.05 μWh·cm^{-2}; cycling retention of 90.7% after 10,000 cycles	[32]
Laser cut	Laser cut kirigami patterning	MXene/bacterial cellulose composite paper	Stretchable MSC arrays; stable under deformation	Areal capacitance of 111.5 mF·cm^{-2}; high areal energy density of 0.00552 mWh·cm^{-2}; stable upon stretching up to 100%	[49]
Laser welding	Light induced plasmonic nanowelding; self-limited by junction geometry	AgNW networks	Self-limited junction welding; localized heating protects low-thermal-budget substrates	Demonstrates self-limited welding concept	[50]
Laser welding	Spatial light modulated femtosecond laser	AgNW network on flexible substrate	Welded nanowire junction network	Sheet resistance down to 14.7 Ω·sq^{-1} with the transmittance of 89.5%; the resistance is slightly increased after 10,000 bending cycles	[35]
Laser reduction	CO_2 laser direct writing; photothermal reduction	Hydrated GO film	RGO–GO–RGO MSC (in-plane/sandwich geometries)	Areal capacitance of 0.51 mF·cm^{-2}; volumetric capacitance of 3.1 F·cm^{-3}; energy density of 4.3 × 10^{-4} Wh·cm^{-3}; cycling retention of 65%–70% after 10,000 cycles	[37]
Laser reduction	Laser reduction of Zn-infiltrated GO	Zn-infiltrated multilayer GO	Multilayer graphene electrode (microstructure tuned by Zn infiltration)	Specific surface area of 378 m^2·g^{-1}; pore volume of 1.72 cm^3·g^{-1}	[38]
Laser irradiation	405 nm direct laser irradiation	GO/V_2O_5·$n$$H_2O$ film	Porous surface; pillarlike protrusions; specific surface area of 17.27 m^2·g^{-1}	Conductivity of 6.8 S·m^{-1}; decreased C–O bonds and O–H functional groups with increasing laser power density	[46]
Laser irradiation	Laser irradiation (defect/oxygen-vacancy engineering)	Ultrafine Co_3O_4 nanoparticles/ graphene	Oxygen-vacancy abundant composite	Specific capacitance of 978.1 F·g^{-1} at 1 A·g^{-1}; cycling retention of 99.3% after 20,000 cycles	[51]

controlling tortuosity and interfacial resistance. They also deliver mechanical compliance (bending, stretching, cyclic strain) and compatibility with hetero-integration (footprint, thermal budget, cleanliness). Laser processing provides the unifying toolkit: by tuning fluence, pulse width, scan strategy, and ambient, it enables top-down patterning (ablation/etching, cutting/scribing) [57], bottom-up formation (sintering/deposition of inks and powders) [58], joining (nanowire and lamina welding) [59], and *in situ* chemistry (photothermal/photochemical reduction, doping, phase/defect and porosity control) [60]. These routes are mapped onto dimensionality to balance areal vs. volumetric metrics and speed vs. fidelity: 1D fibrous/linear formats prioritize long-range conductivity, lineal flexibility, and seamless series/parallel connectivity; 2D thin films exploit planar lithography-like freedom for interdigital layouts and scalable integration while mitigating stacking-induced diffusion limits, and 3D architectures trade process complexity for high loading, hierarchical porosity, and superior volumetric energy density. Accordingly, key device figures of merit (including rate capability, areal and volumetric capacitance, cycling performance, and deformation stability) are correlated by leveraging the laser as a unifying tool for simultaneously tailoring geometry and chemistry.

3.1 One-dimensional architectures

3.1.1 Carbon nanotube (CNT) networks for 1D electrodes

CNTs are 1D nanocarbons that offer exceptional electrical and mechanical properties. Individual CNTs (especially single-walled CNTs) have electrical conductivities approaching 1.04×10^5 S·m^{-1}, and macroscopic CNT fibers or films can achieve metallic-level electrical conductivity, reported to reach 1.1×10^7 S·m^{-1}, about 1/5 that of copper [64, 65]. This high electrical conductivity, combined with inherent flexibility and tensile strength, makes CNT networks a superior choice for electrodes that should endure deformation. For instance, CNT fibers can be woven or braided to form 1D fiber-shaped supercapacitors and flexible cables. In such 1D architectures, CNT fiber electrodes act as both the conductor and active material. Consistent with prior reports, pure CNT electric double-layer capacitor (EDLC) electrodes typically deliver only tens of F·g^{-1} [66, 67] because typical CNT bundles exhibit PET surface areas of only about 10^2 to 10^3 m^2·g^{-1} (e.g., 227.69 m^2·g^{-1} reported by Ramzan et al. [68]). This surface area is markedly lower than that of graphene, and much of the CNT surface is located within bundles or inner walls that remain poorly wetted and thus inaccessible to the electrolyte. Nevertheless, these materials exhibit exceptional structural integrity: CNT films or yarns resist fracture and sustain continuous electrical percolation even under substantial mechanical strain, a behavior that can be attributed to the intrinsic slip and alignment adaptability of individual nanotubes under stress. Cycling stability of CNT-based supercapacitors is typically very high (the retention often exceeding 95% over tens of thousands of cycles) because the carbon material itself is chemically inert in typical electrolytes and does not undergo phase changes [69, 70].

Importantly, CNTs are frequently used as a 1D building block that can be integrated into higher-dimensional architectures. For example, vertically aligned CNT forests (a pseudo-3D structure) can serve as high-surface electrodes, or CNTs can be embedded into polymers to form flexible 2D films. In micro/nano devices, CNTs can be printed as lines or grown *in situ* to form microscopic interconnects or electrodes. They are also frequently combined with pseudocapacitive materials to compensate for the lower intrinsic capacitance. A common strategy is coating a CNT fiber or film with a thin layer of metal oxide or conducting polymer: The CNT network provides a highway for electrons and a resilient mechanical scaffold, while the coating contributes additional Faradaic capacitance. Such hybrids can significantly boost energy storage, as exemplified by CNT/MnO_2 fibers or CNT/MXene coaxial fibers, which exhibit much higher capacitance than bare CNTs at the cost of only a slight trade-off in rate capability [71]. Overall, CNTs play a key role in 1D electrode applications and as flexible connectors, but also play a vital role as conductive additives in 3D composite electrodes due to their ability to bridge particles and prevent restacking (e.g., CNTs inserted between 2D sheets like graphene or MXenes improve ion access and mechanical integrity) [72].

3.1.2 Metal nanowires (CuNWs and AgNWs)

Laser processing has become a key pathway for fabricating 1D metal nanowire electrodes, enabling precise control over junctions, interfaces, and embedding depth while maintaining low thermal budgets. Garnett et al. [50] demonstrated self-limiting welding at AgNW cross-junctions via plasmon-induced local photothermal heating: the naturally occurring nanogaps at the junctions concentrate light to create localized hotspots, and because the heating efficiency is extremely sensitive to the junction geometry, welding self-terminates once contact is made, avoiding thermal damage to surrounding areas. This plasmonic nanowelding enables high-performance interconnect electrodes of AgNW networks on thermally fragile substrates (e.g., plastic films and polymer solar cells) without the need for high-temperature annealing to remove organic ligands. Simultaneously, Lee et al. [62] fabricated ultralong AgNWs and employed low-temperature laser nanowelding to form highly transparent, conductive, and mechanically flexible AgNW networks, as illustrated in Fig. 4(b). The resulting electrodes achieve an optical transmittance of 89%–95% and a sheet resistance of 9 Ω·sq^{-1} (T = 89%) to 69 Ω·sq^{-1} (T = 95%), surpassing the performance of conventional indium tin oxide films. These laser-welded AgNW networks were successfully used in flexible LED circuits and touch panels, highlighting their potential in flexible displays and wearable electronics. As the field advanced, optimization of laser parameters further improved weld quality. Ren et al. [59] focused a nanosecond-pulsed laser on AgNW junctions, leveraging the nanowires' "nanofocusing" effect and plasmonic enhancement to generate localized heating at the nodes and realize self-limiting laser welding; the mechanical strength and electrical conductivity of the welds are comparable to those of pristine nanowires, as shown in Fig. 4(c). They systematically studied the effects of pulse width, fluence, and repetition rate, finding that increasing per-pulse energy while lowering repetition rate (at fixed total energy) confines the heat-affected zone (HAZ) to the vicinity of the junction, thereby improving precision, although excessive energy gradients can introduce thermal stress and defects. With a pulse width of 1 ns and appropriate laser power, AgNWs formed nearly seamless junctions with markedly reduced node resistance, while avoiding the adverse effects of thermal annealing or lamination on flexible devices. The same laser-welding strategies can be extended to other metals, e.g., cost-effective copper nanowires, which exhibit strong surface–plasmon absorption in the visible region, can also be selectively welded/patterned by laser to form high-performance transparent electrodes [73].

Laser processing, likewise, offers distinct advantages for

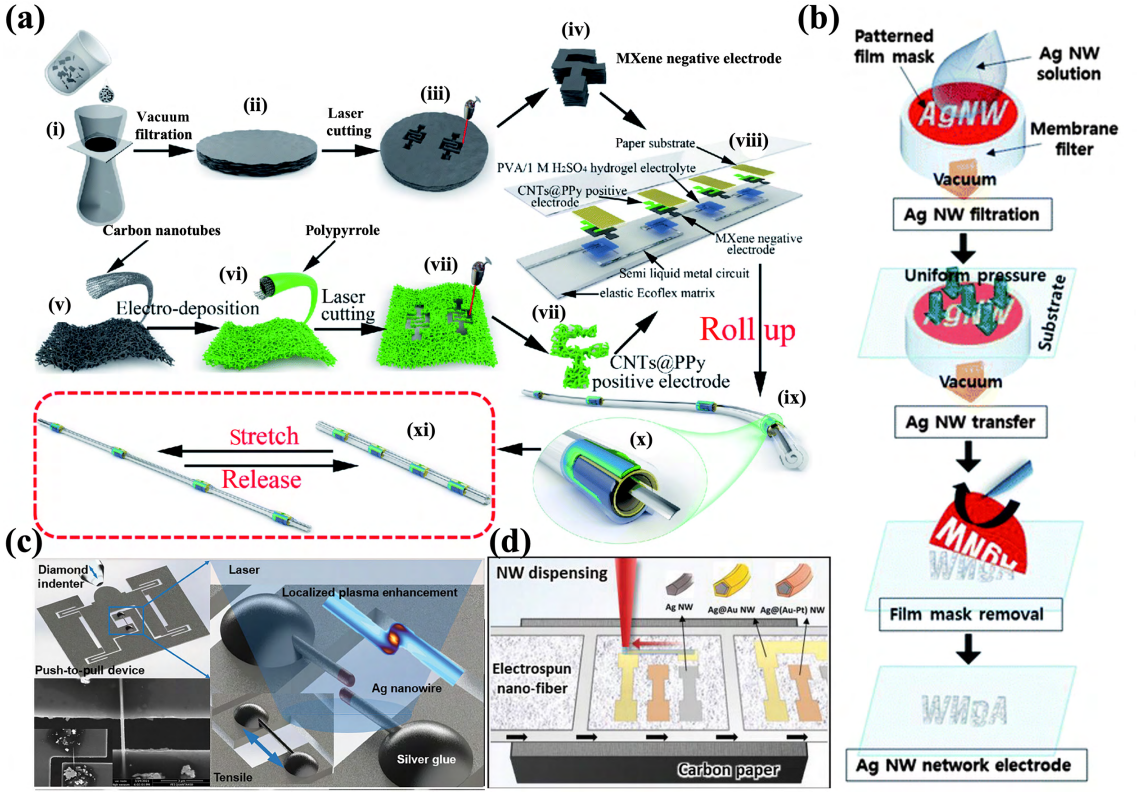

Figure 4 (a) Schematic of the fabrication procedure of the wire-shaped stretchable MSC array based on the rolled-up island-bridge architecture. Reproduced with permission from Ref. [61], © The Royal Society of Chemistry 2021. (b) Schematic diagram of a very long AgNW flexible and transparent conductor fabrication process. Reproduced with permission from Ref. [62], © The Royal Society of Chemistry 2012. (c) *In situ* welding system setup and initial structure of AgNWs. Reproduced with permission from Ref. [59], © Wiley-VCH GmbH 2024. (d) Local filtration-based nanowire printing process on electrospun nanofiber membrane (ENM) utilizing the capillary force of carbon paper. Reproduced with permission from Ref. [63], © Wiley-VCH GmbH 2024.

fabricating 1D electrodes in flexible and bioelectronic devices. Yoon et al. [63] reported a method by which AgNWs are deposited directly by filtration onto an electrospun nanofiber membrane and then post-treated photothermally with a laser (Fig. 4(d)). Using a 532 nm continuous-wave laser raster-scanned at 80–100 mW, the nanowires rapidly convert absorbed light to heat, inducing local melting at the surface of the underlying thermoplastic polyurethane (TPU) fibers; the nanowires thereby become partially embedded in the substrate and welded at their cross-points, forming a robust, conductive embedded network. After laser welding, mechanical stability and adhesion improved dramatically. Even after 80 s of ultrasonication, Ag@Au core–shell nanowires remained firmly adhered and conductive, whereas the printed Ag@Au NWs without laser treatment were almost detached from the substrate immediately upon sonication.

De Chiara et al. [74] used a 355 nm ultraviolet (UV) laser to directly write porous, conductive LIG patterns on polyimide while simultaneously photothermally decomposing a pre-deposited metal-organic framework (MOF) precursor (ZIF-67), forming $Co/Co_3O_4/C$ core–shell nanostructures uniformly embedded in the graphitic matrix. This MOF-derived composite electrode has significantly improved electrochemical performance: compared with unmodified LIG, the interfacial resistance decreased by two orders of magnitude and the areal capacitance increased by nearly 400-fold (2.4 $mF{\cdot}cm^{-2}$ vs. 6 $\mu F{\cdot}cm^{-2}$). The resulting flexible electrodes showed enhanced charge transfer and sensing sensitivity, and also demonstr ated potential as micro-energy-storage electrodes. In summary, by carefully optimizing the laser type (continuous-wave or pulsed), wavelength, and scanning strategy, metal nanowire 1D electrodes can be welded, embedded, and patterned without damaging the substrate, thereby markedly improving conductivity, adhesion, flexibility, and electrochemical performance. These advances provide strong support for the development of flexible electronics, wearable bioelectronics, and next-generation energy storage devices.

3.1.3 Laser-processed 1D electrodes for micro-supercapacitors and biosensors

1D electrodes, such as fibrous and linear ones, could be used in tiny supercapacitors or sensors. Nguyen et al. [75] utilized laser-assisted manufacturing to integrate active electrodes, current collectors, electrolytes, and flexible polymer scaffolds into monofilament fiber supercapacitors. This laser-assisted electrode fabrication method enables the manufacture of series-connected supercapacitors in a seamless monofilament unit without the need for post-manufacturing assembly. Yang et al. [76] reported that laser-treated CNT yarn microelectrodes (CNTYMEs) were employed to improve the sensitivity of dopamine detection. The laser-treated CNTYME maintained higher dopamine sensitivity than the carbon fiber microelectrode while allowing a scan repetition rate of 50 Hz, which is fivefold higher than the conventional frequency. Laser-treated CNTYME exhibits facile preparation, excellent reproducibility, fast electron-transfer kinetics, high sensitivity, and rapid *in vivo* detection of dopamine. Li et al. [61] used the laser cutting technique in the preparation of linear, telescopic MSCs, as shown in Fig. 4(a). They proposed a novel "rolled island bridge

(RIB)" electrode network design to realize a 1D linear telescopic MSC array. Yu et al. [77] manipulated copper nanowire (CuNW) using laser welding combined with dielectrophoresis (DEP) and welded a copper single nanowire for glucose sensing.

3.2 Two-dimensional planar electrodes

3.2.1 Reduced graphene oxide and laser-induced graphene

Graphene-based materials are widely used for micro/nano electrodes due to their excellent electrical conductivity and mechanical flexibility [78]. rGO is typically obtained by chemically or photothermally reducing GO, including laser reduction methods. Some oxygen-containing functional groups are retained in rGO, which are beneficial to surface wettability or further functionalization, while substantially improving electrical conductivity compared with insulating GO. Typical rGO films exhibited electrical conductivity on the order of 10^2–10^3 S·cm^{-1} (e.g., ~ 3×10^2 S·cm^{-1} reported for neat rGO sheets, lower than that of pristine graphene but adequate for microscale electrodes) [79]. Their specific capacitance as pure EDLC materials is moderate (often ~ 100 F·g^{-1} in optimized cases) since charge storage is mainly via surface adsorption rather than Faradaic reactions [80]. However, rGO boasts a very large surface area (theoretically up to 2630 m^2·g^{-1} for single-layer graphene) and can form percolating networks for efficient charge transport [81]. Structurally, rGO films can be fabricated as thin, planar architectures, that are ideal for 2D interdigital electrodes. Indeed, laser-patterned rGO has been used to create planar MSCs on flexible substrates, where the in-plane geometry allows fast ion transport and high-power density.

LIG is a closely related material produced by direct laser writing on precursors like polyimide, which undergoes localized pyrolysis. A graphene-like carbon foam is formed in LIG, with a porous 3D network composed of few-layer graphene nanoflakes [82–84]. This laser fabrication inherently creates a 3D microstructure (with out-of-plane pores and a highly accessible surface area) within a 2D planar pattern. LIG electrodes thus combine high in-plane electrical conductivity with through-thickness porosity for ion diffusion. Their electrical conductivity is high (though slightly lower than defect-free chemical vapor deposition (CVD) graphene, due to the presence of some disordered and functional groups). Crucially, LIG is fabricated *in situ* on the device substrate, ensuring strong adhesion and seamless integration, which is an advantage for structural reliability. For example, Velasco et al. [78] reported a LIG-MSC electrode on polyimide that can achieve an areal capacitance of 22.2 mF·cm^{-2} at 0.05 mA·cm^{-2} with energy and power densities comparable to those of devices employing pseudocapacitive materials, as shown in Fig. 5(b).

From a mechanical perspective, both rGO and LIG are flexible (especially when supported on polymer substrates) and can withstand bending or stress without cracking, making them well-suited for flexible planar devices [85, 86]. In summary, LIG and rGO are ideal for planar electrode architectures, such as interdigital MSCs or sensing electrodes, where a combination of large surface area, excellent electrical conductivity, and strong substrate integration is desired [87, 88]. Their main limitation is primarily in energy density, as their specific capacitance is lower than those of redox-active materials due to their purely carbonaceous nature. Thus, they are typically employed as a conductive scaffold or current collector, sometimes hybridized with coatings to enhance capacitance.

3.2.2 Transition metal carbides/nitrides (MXenes)

MXenes (such as $Ti_3C_2T_x$) have rapidly emerged as promising electrodes, particularly in MSCs and microbatteries (MBs). These are 2D atomic-layer materials obtained by etching MAX phase precursors, yielding flakes that are only a few atoms thick. MXenes combine two key advantages: metallic electrical conductivity and pseudocapacitive surface chemistry. Actually, the electrical conductivity of some MXene films is comparable to those of metals. $Ti_3C_2T_x$ films can reach 10^4–10^5 S·cm^{-1} (on par with titanium metal foil) depending on flake alignment and density [89, 90]. This approach is often superior to that of graphene-based and CNT films via similar fabrication routes, giving MXene electrodes an edge in high-power and high-frequency response. Concurrently, MXene flakes feature abundant surface terminations (–O, –OH, –F) that participate in fast redox reactions with electrolyte ions, enabling faradaic charge storage in addition to double-layer capacitance [91]. The result is exceptionally high capacitance: e.g., $Ti_3C_2T_x$ MXene electrodes have demonstrated specific capacitances of ~ 200–400 F·g^{-1} in aqueous electrolytes [31, 92], and volumetric capacitance of up to ~ 1500 F·cm^{-3} for dense films, which are far above typical carbon materials [93, 94]. Mateen et al. [95] reported that a vanadium carbide MXene (V_2CT_x) delivered ~ 557.7 F·g^{-1} at 1 A·g^{-1}, while Mu et al. [96] reported another MXene/nickel phthalocyanine composite reached 792 F·g^{-1} at 1 A·g^{-1}, highlighting MXenes' capacity for extraordinary energy storage performance.

For micro-scale applications, MXenes can be processed in flexible ways: They form stable colloidal suspensions that can be inkjet-printed or spray-coated into interdigital microelectrode patterns [99, 100]. Planar interdigital MSCs based on MXene films have high areal capacitance. For instance, Yuan et al. [101] proposed the additive-free MXene sediment ink for the construction of MSCs. The proposed MSCs demonstrated a high areal capacitance of 2.337 F·cm^{-2} and an excellent capacitance retention after 10,000 cycles. This work suggests that waste-free MXene, compatible with 3D laser technology, represents a promising strategy for the development of high-performance flexible MSCs suitable for large-scale applications. The primary challenge with MXenes is avoiding restacking of the atomically thin sheets, which can impede ion diffusion between layers [97]. To address this, researchers often introduce nanostructuring or porosity. For instance, laser patterning or chemical etching can create in-plane holes, forming "accordion-like" structures, and can integrate spacer materials, such as CNTs or nanoparticles, to prevent layer restacking [98]. Such strategies yield MXene electrodes that combine high gravimetric and volumetric performance with excellent rate capability.

In summary, MXenes play a pivotal role in the materials landscape, serving as a bridge between pure EDLC carbons and faradaic materials and delivering both high electrical conductivity and high capacitance. They are especially well-suited for planar MSC, where a thin MXene interdigital electrode can outperform carbon-based counterparts in energy density, and they also serve effectively as components in advanced composites for optimized performance.

3.2.3 Laser-processed 2D electrodes

With the continuous development of portable and wearable micro-electronic devices, various components tend to be miniaturized and flexible. This presents both opportunities and challenges for 2D thin-film or planar electrodes. At present, state-of-the-art materials

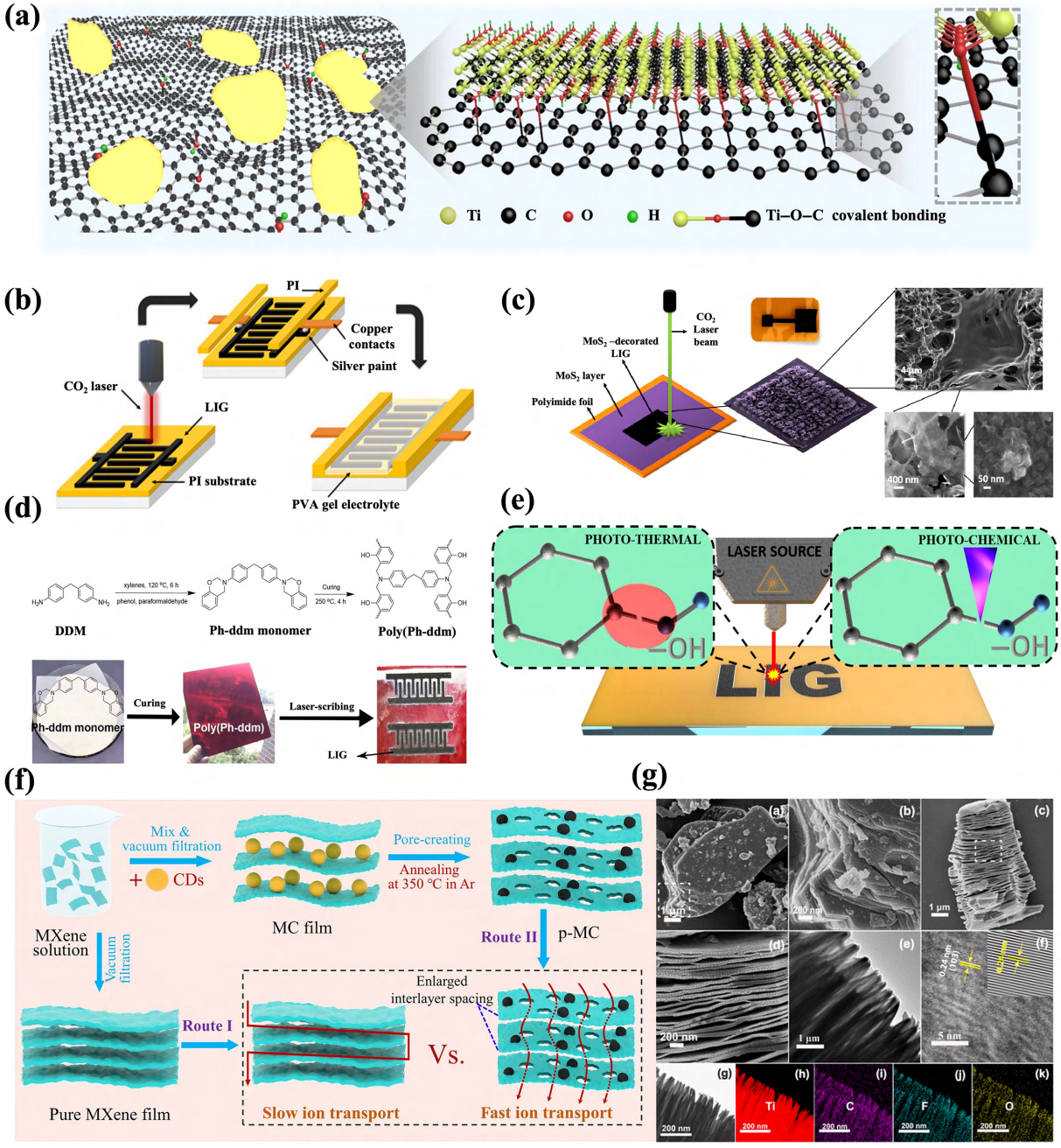

Figure 5 (a) Schematic model of MXene-GO platelets showing the formation of Ti–O–C covalent bonding. Reproduced with permission from Ref. [79], © Zhou, T. Z. et al. 2020. (b) Schematic drawing of the laser setup that was constructed to irradiate the polyimide. Reproduced with permission from Ref. [78], © Velasco, A. et al. 2023. (c) 3D scheme of the laser-writing process onto MoS_2-covered polyimide foil and field emission scanning electron microscopy (FESEM) images at different magnifications, showing the morphology of the MoS_2-decorated LIG. Reproduced with permission from Ref. [85], © American Chemical Society 2016. (d) Schematic illustration for the preparation of poly(bis(4-(2H-benzo[e][1,3]oxazin-3(4H)-yl)phenyl)methane)-based LIG. Reproduced with permission from Ref. [86], © Elsevier Ltd. 2020. (e) Laser scribing on a PI sheet using the photothermal and photochemical process. Reproduced with permission from Ref. [87], © Elsevier Ltd. 2023. (f) Schematic illustration of the fabrication process of porous MXene (p-MC) film and the advantages of p-MC film over traditional pure MXene film. Reproduced with permission from Ref. [97], © Wang, Y. B. et al. 2023. (g) FESEM images of accordion-like multilayered 2D $Ti_3C_2T_x$ MXene. Reproduced with permission from Ref. [98], © American Chemical Society 2022.

employed in the fabrication of planar MSCs include graphene, transition metal oxides/hydroxides, transition metal dihalides, metal carbides, metal nitrides, etc. [102]. The most common types are MXene thin-film structures, graphene films, other metal compound films, and carbon plates.

Since their discovery in 2011, MXene thin films have attracted considerable attention due to their hydrophilic nature, excellent electrical conductivity, and ease of mass synthesis in scalable processes [103]. MXene thin film used in energy storage devices is gradually developing towards a flexible and integrated direction. Jiao et al. [49] fabricated a unique composite structure using 2D fully delaminated few-layered $Ti_3C_2T_x$ MXene flakes and 1D bacterial cellulose (BC) fibers, as shown in Fig. 6(a). The mechanical strength is improved while the overlap area is enlarged, and the

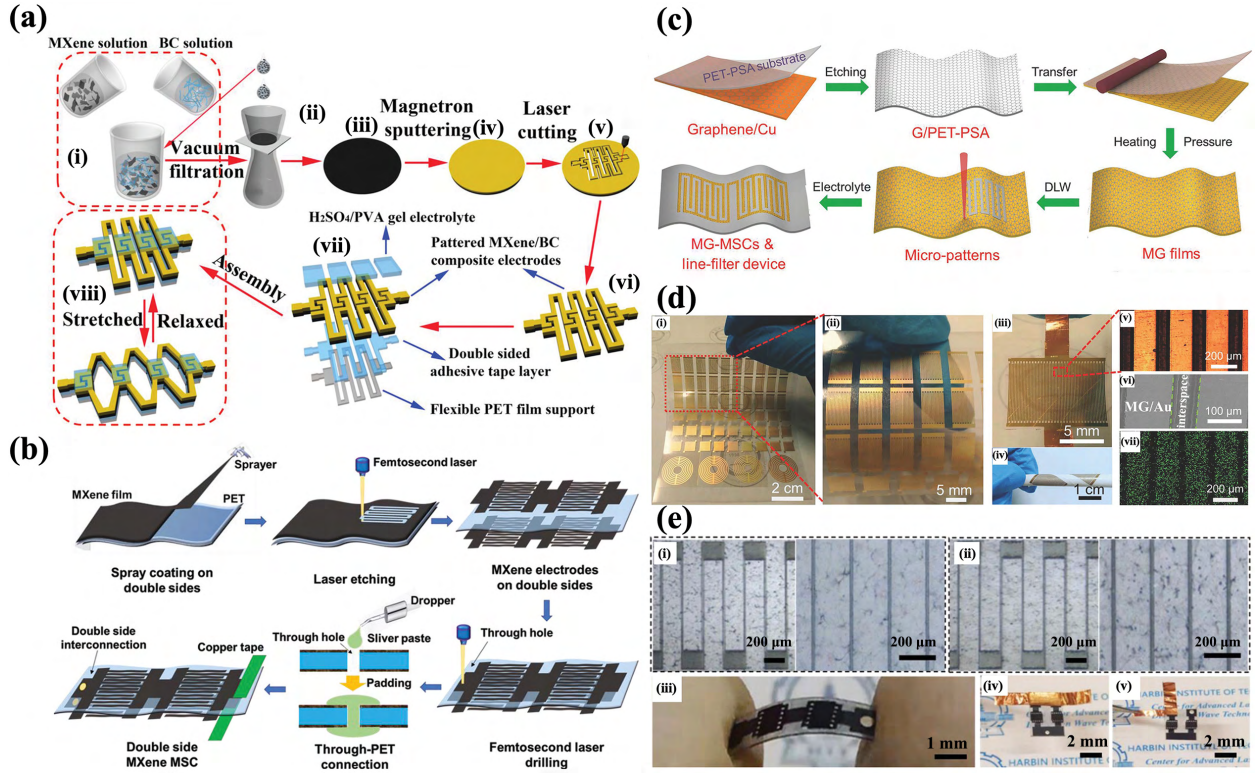

Figure 6 (a) Flowchart of the protocol for preparing MXene/BC composite papers and their kirigami patterning with laser cutting for all-solid-state stretchable MSCAs. Reproduced with permission from Ref. [49], © Jiao, S. Q. et al. 2019. (b) Fabrication and images of MXene double-side MSCs (DSMSCs) on PET substrate. Reproduced with permission from Ref. [106], © WILEY-VCH Verlag GmbH & Co. KGaA, Weinheim 2020. (c) and (d) Facile electrode design of solid-state flexible multilayered graphene–MSCs using transferred CVD graphene films. Reproduced with permission from Ref. [108], © WILEY-VCH Verlag GmbH & Co. KGaA, Weinheim 2018. (e) Images of MXene DSMSCs on PET substrate. Reproduced with permission from Ref. [106], © WILEY-VCH Verlag GmbH & Co. KGaA, Weinheim 2020.

contact resistance is reduced. After that, femtosecond laser machining technology was used to fabricate an interdigital electrode with a small spacing. The composite electrode achieved the stretching, twisting, and bending of an all-solid MSC with high regional capacitance and high regional energy density. Molybdenum disulfide was incorporated into MXene to obtain enhanced energy density [105]. The schematic illustration of the fabrication process is presented in Fig. 6(a). In addition, Li et al. [106] prepared MXene films by spraying them on both sides of the PET substrate (Fig. 6(b)). The transparency of the PET substrate allowed simultaneous laser etching of the MXene films on both sides without damaging the substrate. Notably, the laser focus should be positioned at the mid-thickness of the PET substrate during processing to ensure uniform etching quality on both sides. Then, an MSC with serial or parallel connections was prepared by injecting silver slurry onto PET using laser drilling technology. The specific production process and processing results are shown in Fig. 6(b). Post-characterization revealed that the transverse distance of the thermally affected region of MXene after processing was within one micron due to the small thermally affected region of femtosecond laser processing. This double-sided configuration provides enhanced integration.

Graphene can also be integrated into thin film structures, but high-resolution printed graphene circuits still face a technology shortage. It can be improved by using inkjet maskless lithography in reference to the study of Hondred et al. [107]. In terms of flexibility, graphene thin-film electrodes are partially limited by stacking. To address this limitation, Choi et al. [109] achieved an increase in capacitance by ablating, stripping, and modifying graphene surfaces with nanosecond pulsed lasers. In addition, an increasing number of researchers have adopted LDW for the patterning of graphene films. Ye et al. [108] further exploited the flexibility of LDW to fabricate graphene films with diverse planar geometries, as shown in Figs. 6(c) and 6(d). In particular, Gao et al. [110] innovatively proposed a unique LDW strategy, which can realize the production of MSCs with different dimensions. Shi et al. [111] developed a process for stacking multilayer thin-film structures on liquid substrates, which opens new possibilities for 3D manufacturing.

Besides the two materials mentioned above, conventional materials have also been explored for planar electrodes. For example, a porous carbon electrode was prepared by light-assisted processing [112]. For metal, Lee et al. [113] fabricated a flexible supercapacitor based on a nanoporous silver layer by laser induction, which has excellent performance of high energy density and high power density. In addition, the preparation of thin film electrodes based on MFe_2O_4 (M = Mg, Zn), $LiCoO_2$, $CsPbBr_3$, and other metal compounds have also been developed [112, 114, 115].

3.3 Laser-processed three-dimensional electrode architectures

The development of high-performance and miniaturization of MSCs is an inevitable trend in the era of intelligence. The demand for micro power supply devices in applications such as the IoT and intelligent healthcare has prompted widespread interest in MSCs. To meet the evolving demands of MSCs, researchers leveraged the high precision, spatial resolution, and design flexibility of laser

processing to construct a 3D electrode structure, thereby enhancing the achievable energy density of MSCs [116, 117]. The 3D structure of MSC has been explored mainly from the aspects of array, protuberance structure, or sag structure [118, 119].

Back in 2017, Lee et al. [120] innovatively proposed printing microcone arrays on metal electrodes. The schematic diagram and results are shown in Fig. 7(a). The microcone arrays have since been applied to photosensitive resin systems for 3D printing [121]. Initially, the microelectrode array is designed using 3D software, after which the basic structure is fabricated via laser 3D printing. Special attention should be paid to the printing process, in which the equipment should be printed at an angle of 45° in the horizontal direction, so as to facilitate separation. Then, metallization, lamination, packaging, electroless microporous platinum plating, and laser processing were used to obtain a microelectrode array (MEA) (Fig. 7(b)) [122]. The electrical, electrochemical, and hydration stabilities of 3D MEAs fabricated by this method were comparable to those of devices produced using more sophisticated and costly fabrication techniques. Subsequently, a micropillar array architecture was developed to further enhance performance. Chen et al. [123] produced a polydimethylsiloxane (PDMS)-based micropillar electrode array coated with gold films using a two-step soft lithography process. Electrochemical characterization revealed that the array significantly enhanced the voltammetric current density. The two most commonly used approaches for introducing pits in microelectrode architectures are porous and grooved structures.

The performance of the microelectrode can be effectively enhanced by forming surface concavities via this method. Kim et al. [124] used photolithography to fabricate MSCs based on porous carbon from top to bottom. The incorporation of boron effectively enhanced the capacitor's performance. Figure 7(d) illustrates the detailed fabrication process along with the corresponding SEM images. However, employing porous structures introduces challenges related to the intrinsic brittleness of the materials and the limited rate capability of graphene electrodes. For the problem of fragility, Li et al. [125] first filled porous electrode with gel electrolyte before using laser ablation to make microelectrodes, forming a new electrode structure. The filled gel electrolyte can serve not only as a binder to improve the mechanical performance of the material, but also as an ion-storage layer and a diffusion channel, thereby optimizing the electrochemical performance. For the problem of rate limitation, a 3D hierarchical porous structure dominated by meso-and macro-porous structures can be adopted, instead of the micropore-dominated electrode structure [16]. In addition to introducing porosity, creating grooved structures can also improve the electrochemical performance of the electrode. Cho et al. [126] fabricated patterned Si film containing trench-structured Cu current collectors by combining laser printing and electrochemical etching techniques. Two forms of silicon coating are employed: full coverage and selective coverage, where the coating is confined to the trench bottom. Experiments showed that both configurations could enhance the electrode capacity, but the latter exhibited a more pronounced effect. In addition, they explored the geometry of the grooves when they showed optimal electrochemical performance.

In addition to the two aforementioned 3D configurations, a unique 3D electrode design has also been developed. It integrates 80 thin-film electrodes across ten flexible polymer probes, forming a 3D MEA. Although the device is fabricated from thin-film structures, the hinge region of each probe can plastically deform and be peeled off the plane, enabling it to function as a 3D microelectrode. This innovative achievement was successfully applied in electrically interrogating 3D *in vitro* cultures of

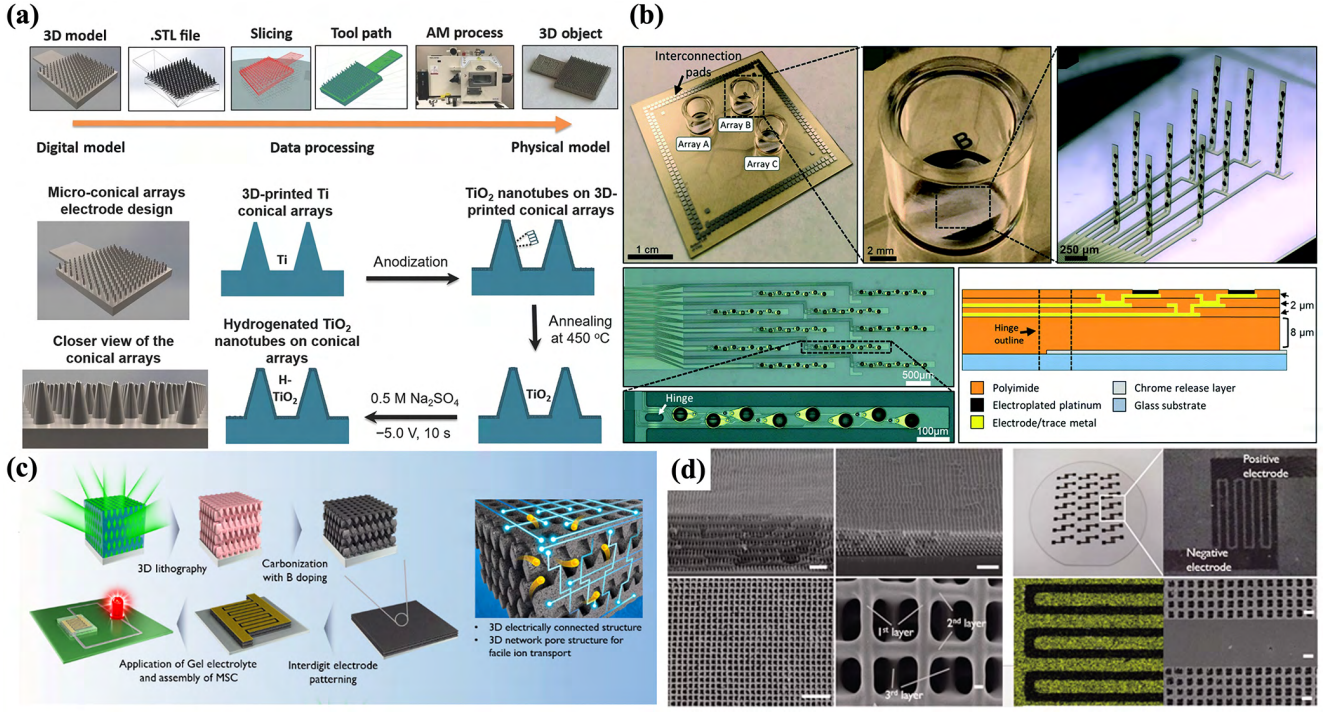

Figure 7 (a) Fabrication of 3D-printed micro-conical electrodes and functionalization with hydrogenated TiO_2 nanotubes for electrochemical applications. Reproduced with permission from Ref. [120], © WILEY-VCH Verlag GmbH & Co. KGaA, Weinheim 2017. (b) 3D MEA device prior to actuation. Reproduced with permission from Ref. [122], © Royal Society of Chemistry 2020. (c) Schematic fabrication of the boron-doped 3D porous carbon patterned interdigital microelectrodes and their all-solid-state MSCs and (d) SEM and EDX analysis of 3D-printed porous carbon electrodes. Reproduced with permission from Ref. [124], © Elsevier Ltd. 2018.

electroactive cells. The specific structure and application are shown in Fig. 7(b) [122].

3.4 Mechanism of laser processing across 1D, 2D, and 3D

The previous sections summarized representative laser processing methods (additive, subtractive, joining, and chemical conversion) and device demonstrations. Laser microfabrication is a facile energy input approach and a mechanism-oriented process by which different laser-induced phenomena are deliberately achieved, and electrode performance is optimized. Instead of using the laser merely to deliver heat or ablate material, researchers investigated multiple mechanisms, such as welding, sintering, ablating, annealing, and surface activation, either sequentially or simultaneously [127]. These strategies feature the laser's exceptional versatility. By tuning laser parameters, a single laser system can synthesize materials (e.g., forming LIG or reducing metal precursors), pattern or ablate structures with micro- to nanoscale precision, and even modify interfaces or chemistry *in situ*. By choosing the appropriate mechanism (or combination of mechanisms) at each dimension (1D, 2D, and 3D), one can tailor the electrode architecture and interfaces to achieve an optimal balance between electrical continuity, interfacial integrity, and mechanical resilience. Table 2 provides a dimension-dependent overview of fabrication complexity, typical materials, and integration levels, as a guide discussing mechanisms and trade-offs.

3.4.1 1D

In 1D micro/nano electrodes, laser-welding has been used to obtain joint nanostructures and ensure continuous electrical percolation along the length, while minimizing the addition of binders or links. For instance, ultrafast laser nanowelding of silver nanowire networks melts and fuses their junctions, dramatically reducing resistivity and contact resistance without damaging flexible substrates. This laser-welding strategy enhances both electrical conductivity and reliability, resulting in nanowire films with highly uniform sheet resistance that can withstand thousands of bending cycles with negligible performance degradation. Such laser-welded 1D conductors can serve as stretchable interconnects or fiber-shaped electrodes. Additionally, mild laser annealing can be scheduled after welding or deposition to relieve stress and heal defects in 1D materials, further enhancing electrical conductivity and flexibility. As a result, combining "welding + light annealing" in 1D electrodes yields continuous electron pathways with improved robustness. For example, laser-treated CNT yarns and nanowire filaments show higher electrochemical performance (e.g., faster electron transfer and higher dexterity in sensors) than their untreated counterparts, because of the removal of surface residues and the creation of cleaner, bonded junctions [128].

3.4.2 2D

In 2D microelectrode films or patterns, a single laser process can accomplish multiple tasks in one workflow. LDW (e.g., scribing a film to form interdigital electrodes), combined with laser drilling of via-holes or pores and subsequent laser cleaning of debris, enables the fabrication of high-performance planar microelectrodes. This "direct write + drill + clean" approach has been demonstrated in MSC fabrication. For instance, Wang et al. [104] fabricated an ultrastretchable MXene microsupercapacitor by transferring an MXene/Au composite film onto a prestrained elastomer substrate, followed by selective laser patterning into an interdigitated structure. The resulting device delivered a high areal capacitance of about 185 mF cm^{-2} and maintained stable operation under strains up to 800% area strain. In another example, Li et al. [106] spray-deposited MXene on both sides of a PET substrate and simultaneously laser-patterned the MXene films on each side by focusing a femtosecond beam in the middle of the transparent sheet. They then used laser drilling to open microvia holes and filled them with electrically conductive silver paste, effectively connecting the two patterned layers in series or parallel. Such multi-step laser processing yields planar electrodes with through-plane connections and minimal parasitic resistance. Following patterning and drilling, an optional low-power laser scan or a solvent rinse can be used to remove charred residues and surface oxides, thereby cleaning the electrode surfaces and ensuring high interfacial quality for subsequent electrolyte coating or device packaging. Overall, by combining planar laser writing, perforation, and post-process cleaning, 2D microelectrodes can achieve finely controlled geometries (short in-plane ion paths) while maintaining excellent interface contact and structural integrity required for device integration.

3.4.3 3D

3D electrodes benefit from hybrid laser strategies that construct material while carving channels, thereby integrating additive and subtractive modes within a single process. In practice, this might involve layer-by-layer laser sintering/deposition to construct thick or high-aspect ratio features, coupled with laser texturing (ablation) to introduce porosity or patterns within and between layers. For example, Do et al. [130] used a laser additive-subtractive

Table 2 Dimension-dependent qualitative comparison of laser-processed micro/nano electrodes

Dimension	Fabrication complexity	Typical materials used	Application and integration level
1D (fibers/lines/yarns)	Low-medium Single-pass welding [77]; cutting [61]	CNT film; AgNW/CuNW (laser-welded) [35]; LIG microribbons on fibers [111]	High for textiles/filaments Monofilament power fibers [75]; stretchable interconnects [71]; easy series/parallel along length
2D (planar films/ interdigital)	Medium Mask-free direct writing [107]; micro-perforation/cleaning [129]; double-sided patterning needs precise focus [106]	rGO (laser-reduced GO), LIG on PI; MXene inks/films (inkjet/spray + laser) [101]; graphene/CNT hybrid films; metal thin films [102]	BEOL-friendly planar integration Interdigital layouts [87, 88]; facile on flexible PET/PI [108]; good routing to ICs/sensors
3D (pillars/cones/porous structures/grooved structures)	High Additive–subtractive combos [130]; layer-wise sintering + texturing [127]; thermal management critical [60]	LIG foams/porous carbons [124]; MXene-infiltrated scaffolds [75]; CNT-reinforced frameworks [33]; metal current collectors (laser-deposited/etched) [131]	Monolithic 3D integration Thick loading with engineered channels [127]; trench/via connection to collectors [126]; suitable for high-density micro-power or MEAs [123]

microfabrication route to create 3D MSC electrodes. Laser-directed metal deposition was used to print 3D current collectors, and subsequent laser etching sculpted well-defined microgroove–plateau structures in the active material. The resulting electrodes had an interconnected framework that significantly enhanced electrolyte accessibility and ion transport. Similarly, in thick battery cathodes, femtosecond laser grooving (ablating an array of vertical channels into a slurry-cast Li-ion electrode) provides shorter ionic diffusion distances across the electrode thickness. Zhu et al. [127] showed that such laser-generated 3D electrolyte channels in an NMC622 cathode led to much more uniform Li^+ distribution and utilization, enabling a threefold increase in high-rate capacity (areal capacity retention about 70% at ~ 1.15 C, versus ~ 23% for an unstructured thick cathode). Notably, the laser-textured 3D electrode also suppressed detrimental lithium plating and improved cycle life. This highlights the capability of subtractive texturing combined with layer-wise sintering, through which the laser can create hierarchical porosity and robust interlayer bonding in tandem. Iterative cycles of deposition and ablation enable the fabrication of 3D electrodes that combine high active mass loading and enlarged surface area for enhanced energy density, with efficient ion/electron transport pathways and robust interfacial integrity ensuring long-term stability.

In summary, mechanism-informed laser processing enables dimension-specific fabrication strategies, including welding or annealing for 1D fibers, direct-write patterning with subsequent drilling and cleaning for 2D films, and surface texturing combined with layer-by-layer sintering for 3D architectures. This design yields micro/nano electrodes that are not only high-performance (simultaneously high areal/volumetric energy and high power) but also highly reliable. By ensuring continuous conductive networks, optimized ion channels, clean interfaces, and mechanical compliance, such laser-fabricated electrodes deliver an optimized balance across critical performance metrics. Importantly, the laser's flexibility as a single tool for multi-step processing is what enables this "from energy input to mechanism orchestration" paradigm shift [132]. As recent reviews emphasize, advancing laser-based multiscale fabrication will be pivotal for next-generation integrated micro power devices [130]. The continued development of mechanism-aware laser strategies that precisely coordinate ablation, sintering/welding, and chemical modification is expected to enable high-energy, high-power, and durable micro/nano electrodes for future flexible and miniature electronics.

To enable quantitative benchmarking across dimensional architectures, Table 3 summarizes representative 1D/2D/3D electrodes with (i) structure descriptors, (ii) key electrochemical metrics (capacitance/capacity where available), and (iii) cycling/reliability indicators.

4 Applications of the multi-functional and highly reliable electrode for heterointegrated devices

4.1 Laser-processed electrodes in supercapacitor applications

In the era of information and intelligent technologies, nearly all devices used in modern production and daily life rely on energy storage components. The most fundamental of these are capacitors and inductors. The difference is that the energy in the inductor is stored as a magnetic field, while the energy in the capacitor is stored as an electric field. Supercapacitor storage is more widely used because of its lower energy loss, smaller volume and weight, faster charging and discharging, and virtually infinite cycle life, in contrast to inductive storage [133]. Especially in recent years, MSCs are developing towards the direction of higher capacitance and energy density, greater miniaturization [134] and enhanced flexibility. Rechargeable energy storage devices represented by MSCs have witnessed remarkable growth [135, 136]. To achieve high capacitance and energy density, lasers can be used for drilling or surface machining.

In parallel with MSCs, laser-enabled microfabrication has also rapidly advanced MB technologies (e.g., laser-patterned zinc-based MBs and high-energy flexible aqueous Zn MBs), where laser-defined architectures play a vital role in enhancing ion/electron transport and device integration [135–137]. For example, 3D architecture engineering has been reported to improve the high-rate performance of aqueous Zn–Mn MBs, highlighting the broad relevance of laser processing for micro-energy storage devices [117].

4.1.1 Laser-modified composite electrodes

Anchoring of these oxygen vacancies on graphene effectively promotes charge transfer and significantly enhances the electrochemical performance of the MSCs [138, 139]. Yang et al. [51] produced oxygen vacancies and ultrafine Co_3O_4 nanoparticles/graphene (UCNG) composites by laser irradiation. Experimental and calculation results reveal that laser irradiation induces abundant oxygen vacancies on the surface of Co_3O_4 nanoparticles in this composite. Fixation of these oxygen vacancies on graphene effectively promotes charge transfer and significantly enhances the electrochemical performance of the MSCs. In addition to Co_3O_4, zinc oxide and other metal oxides can also be employed to achieve similar improvements [138, 140]. In particular, Pazhamalai et al. [146] prepared a unique asymmetric supercapacitor (ASC) using a mass ratio of copper tungsten sulfide/Ni (CWS/Ni) and graphene of about 1:2. The electrochemical investigation of the CWS/Ni||graphene ASC suggests the superior charge-storage property with a high specific capacitance (107.9 $F{\cdot}g^{-1}$/226.67 $mF{\cdot}cm^{-2}$), an elevated energy density (48.57 $Wh{\cdot}kg^{-1}$/102 $\mu Wh{\cdot}cm^{-2}$), and excellent cyclic stability over 10,000 cycles.

4.1.2 Laser-processed micro-supercapacitors

Lasers are used to manufacture MSCs, primarily for graphene. Flat capacitors are available [147], but more flexible film capacitors are available. With the continuous development of flexible wearable devices, energy storage devices face opportunities and challenges. Flexibility, integration, structural and functional diversity, and high performance are required in such energy storage devices [85, 110, 148]. This has aroused widespread concern among researchers. As illustrated in Figs. 8(a)–8(c), graphene MSCs were fabricated via laser irradiation. By leveraging the flexibility, low cost, and convenience of laser processing, Xu et al. [149] prepared a flexible, patternable MSC based on graphene modified by metal oxide (e.g., Co_3O_4). This patterned MSC exhibited a high areal capacitance of 10.9 $mF{\cdot}cm^{-2}$ and excellent stability above 97.8% after 10,000 cycles, and further demonstrated excellent flexibility and good stability under different bending states, outstanding extensibility, and strong integration capability.

In addition, Yuan et al. [145] used space-shaped femtosecond

Table 3 Dimension-dependent quantitative benchmarking of laser-processed micro/nano electrodes (1D/2D/3D)

Dimension	Representative architecture/system	Structure characteristics	Key electrochemical/ functional metrics	Cycling stability/reliability	Ref.
1D	LIG + MOF-derived flexible electrode	Laser induced porous graphene with embedded Co/Co_3O_4/C core–shell nanoparticles	Areal capacitance of 2.4 mF·cm^{-2} (about 400× higher than bare LIG); interface impedance reduction by two orders of magnitude	Flexible sensing with enhanced charge transfer; cycle life not quantified	[74]
1D	Laser-assisted monofilament fiber supercapacitor	Laser-patterned microscale current collectors and active electrodes on a polymer monofilament	Specific capacitance of 24.5 mF·cm^{-2} at 0.1 mA·cm^{-2}	94.3% of capacitance retention after 3000 bending cycles	[75]
1D	Weldable graphene ribbon@Ni fiber all-solid-state supercapacitor	Flexible fiber electrode with weldable architecture (graphene ribbon@Ni)	Length capacitance of 73.8 mF·cm^{-1} at 2 mV·s^{-1}; 26.8 mF·cm^{-1} at 200 mV·s^{-1}	80% of capacitance retention with the length of the electrode from 1.0 to 10.0 cm; 82% of capacitance retention after 10,000 cycles	[141]
2D	LIG MSC	Porous 3D network created via laser writing on polyimide	Areal capacitance of 22.2 mF·cm^{-2} at 0.05 mA·cm^{-2}; energy density of 3.07 μWh·cm^{-2}; power density of 0.0462 mW·cm^{-2}	High flexibility and strong adhesion; cycling stability not explicitly reported	[78]
2D	$Ti_3C_2T_x$ MXene–Prussian Blue MSC	Planar film of MXene blended with Prussian Blue via lift-off	Areal capacitance of 93 mF·cm^{-2} at 2 mA·cm^{-2}; retains 40 mF·cm^{-2} at 100 mA·cm^{-2}; energy density of 45.3 μWh·cm^{-2}; power density of 28.4 mW·cm^{-2}	89% of capacitance retention after 10,000 cycles	[142]
2D	Metal-free MXene MSC on paper substrates	Footprint area of 20 mm^2 (on-paper integration)	Areal capacitance of 5.7 mF·cm^{-2}; areal energy density of 12.05 μWh·cm^{-2}	> 95% of capacitance retention after 10,000 cycles at 1000 mV·s^{-1}	[143]
3D	Temporally and spatially shaped femtosecond laser-based maskless fabrication architecture for multitype planar MSCs on 1T-MoS_2/MXene thin films	3D micropatterned electrode (resolution: ~ 10 μm; precision: 200 nm)	Specific capacitance of 220 mF·cm^{-2}; volumetric capacitance of 1101 F·cm^{-3}; energy density of 0.495 Wh·cm^{-2}; peak power density of 28 kW·cm^{-2}	98.3% of capacitance retention after 15,000 cycles	[144]
3D	Space-shaped femtosecond laser/laser photonic-reduction stamping micro-supercapacitor (3D LIG-based electrode)	3D LIG-based electrode; narrow gaps down to 500 nm; > 30,000 MSCs within 10 min	Energy density 0.23 Wh·cm^{-3}; specific capacitance 128 mF·cm^{-2} and 426.7 F·cm^{-3}	Capacitance retention up to 75.5% when the scan speed increased from 50 to 1000 mV·s^{-1}	[145]
3D	Laser-ablated 3D microelectrodes from gel-infused thick porous electrodes	Gel electrolyte infused porous electrode film; laser ablation enables 3D high-aspect-ratio microelectrodes; thickness up to 260 μm; mass loading up to 13 mg·cm^{-2}	Areal capacitance up to 4640 mF·cm^{-2}; areal energy density of 1318 μWh·cm^{-2}	97% of capacitance retention after 10,000 charging–discharging cycles at 10 mA·cm^{-2}	[125]

laser (SSFL) to induce the generation of high-performance MSCs with 3D spatial structure on a graphene base. This study used a femtosecond laser to synthesize LIG/MnO_2 composites through a reduction–oxidation route and simultaneously form a porous 3D architecture, as shown in Figs. 8(a)–8(c). As a result, the areal and volumetric capacitances increased to 128 mF·cm^{-2} and 426.7 F·cm^{-3}, respectively. In addition, as 1000 space-shaped laser pulses can be generated in one second, more than 30,000 miniature MSCs can be produced in 10 min, enabling batch processing. This approach alleviates the limitations of low processing efficiency and low energy density to a certain extent, thereby promoting the further development and applications of MSCs in the field of energy storage. Moreover, this method can be applied to a variety of materials. Shi et al. [111] also creatively processed and fabricated graphene microribbons on liquid surfaces. Beyond single-cell MSC demonstrations, recent device-level integration has achieved much higher output voltages through tandem architectures. Liu et al. [150] reported 3D graphene paper-based tandem metal-free thin-film supercapacitors with an integrated output up to 200 V, highlighting the importance of architecture and interconnect design for practical micro-power integration.

4.2 Laser-processed electrodes in energy conversion devices

Electrodes also have applications in energy conversion devices, such as thermoelectric materials in thermoelectric power generation devices, electrodes in solar cells, and electrocatalytic electrodes. Recent progress shows that binder-free electrocatalytic electrodes can be constructed using lasers. Sha et al. [151] demonstrated a laser-induced hydrothermal reaction route to rapidly grow catalytic nanostructures for water splitting, providing a promising pathway toward scalable fabrication of high-performance electrocatalytic electrodes with controlled interfaces. In a broad sense, the energy conversion material responsible for energy–electricity conversion in

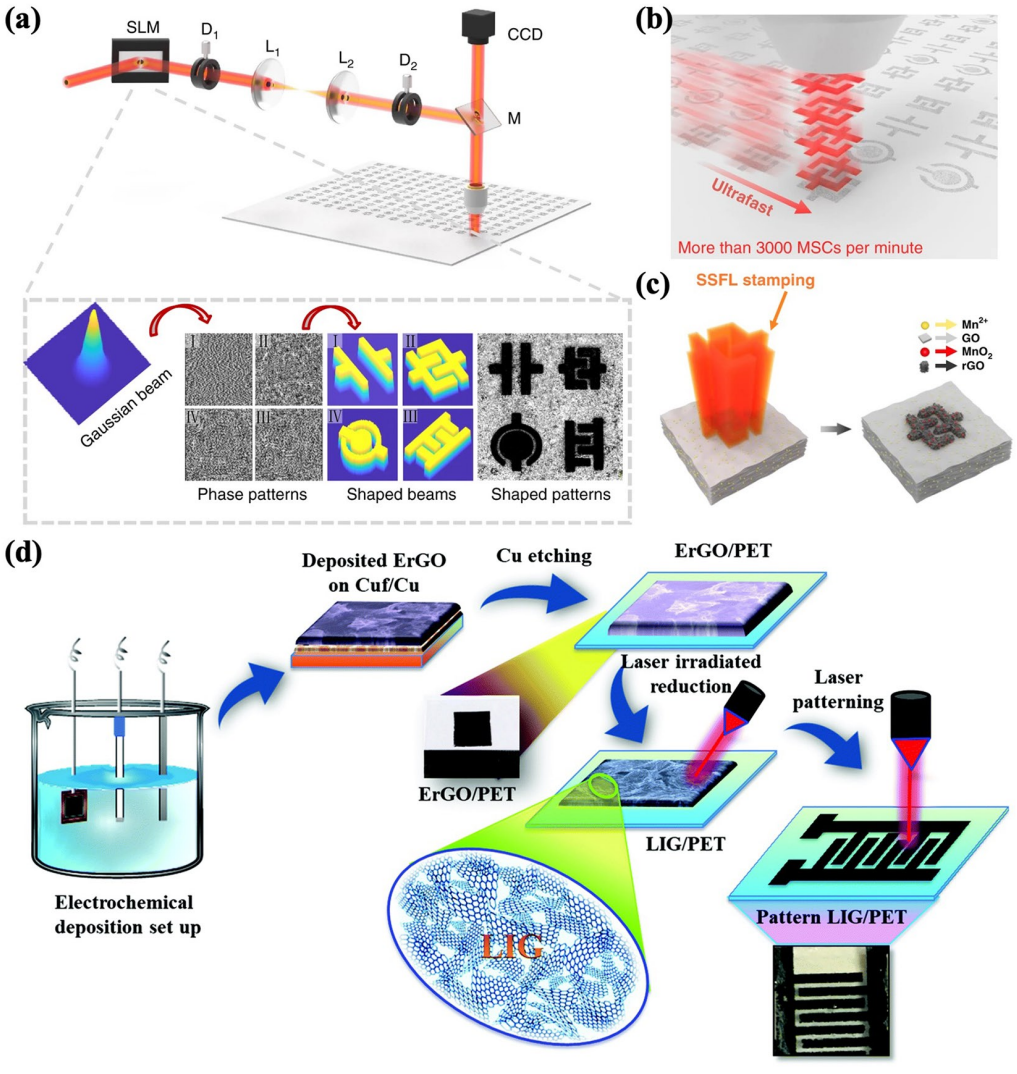

Figure 8 (a)–(c) Schematics of spatially shaped femtosecond laser (SSFL) strategy to fabricate the graphene/MnO_2 MSCs. Reproduced with permission from Ref. [145], © Yuan, Y. J. et al. 2020. (d) Schematic representation of the electrochemical synthesis followed by laser-irradiated reduction used for the preparation of LIG-MSC. Reproduced with permission from Ref. [148], © The Royal Society of Chemistry 2019.

such devices can be considered equivalent to electrodes, e.g., the P-type and N-type thermoelectric materials in thermoelectric generators. Kim et al. [152] fabricated a high-performance flexible thermoelectric generator (F-TEG) using screen printing technology (SPT) and laser multiple scanning technology (LMS), as illustrated in Figs. 9(a)–9(c). The F-TEG module has an output power density of 4.78 $mW{\cdot}cm^{-2}$ at a temperature difference of 25 °C and has considerable flexibility and mechanical stability. Yan et al. [153] successfully prepared bulk ZrNiSn samples on titanium substrates by combining self-propagating high-temperature synthesis (SHS) and selective laser melting (SLM). ZrNiSn, based on SLM, is a promising new thermoelectric material. Using this approach, ZrNiSn was printed on a titanium substrate for the first time, achieving a one-step fabrication of the thermoelectric strut. This work lays an essential foundation for future studies aimed at manufacturing ZrNiSn-based modules by SLM and extending the technology to other thermoelectric materials. Wu et al. [157] integrated non-contact dispensing printing with selective laser melting (SLM) to achieve rapid, straightforward, and cost-effective fabrication of Bi_2Te_3 bulk samples. Zhang et al. [158] employed a laser-induced recrystallization approach during the fabrication of ultra-long, single-crystalline SnSe fibers possessing a rock-salt structure and excellent thermoelectric performance, thereby converting the SnSe cores into single-crystalline structures along the entire fiber length. The single-core or multi-core SnSe fibers manufactured by this method not only exhibit high thermoelectric properties but also high mechanical flexibility and stability, making them suitable for a wide range of applications, including exceptionally flexible and wearable thermoelectric electronics. Chen et al. [159], for the first time, designed thermoelectric composite films composed of well-oriented $(Bi, Sb)_2Te_3$ (BST) nanocrystals and randomly dispersed diamond-like clusters on SiO_2/Si substrates by double-beam pulsed laser co-deposition technique. The significantly enhanced Seebeck coefficients up to 550 $\mu V{\cdot}K^{-1}$ and the corresponding power factor of ~ 46 $\mu W{\cdot}cm^{-1}{\cdot}K^{-2}$ were comparable with or higher than previously reported values of BST or BST-based nanocomposites.

In addition, solar cells are also typical energy conversion devices. Chen et al. [160] introduced the femtosecond laser annealing (FS-LA) process into the preparation of ink-printed $Cu(In,Ga)Se_2$

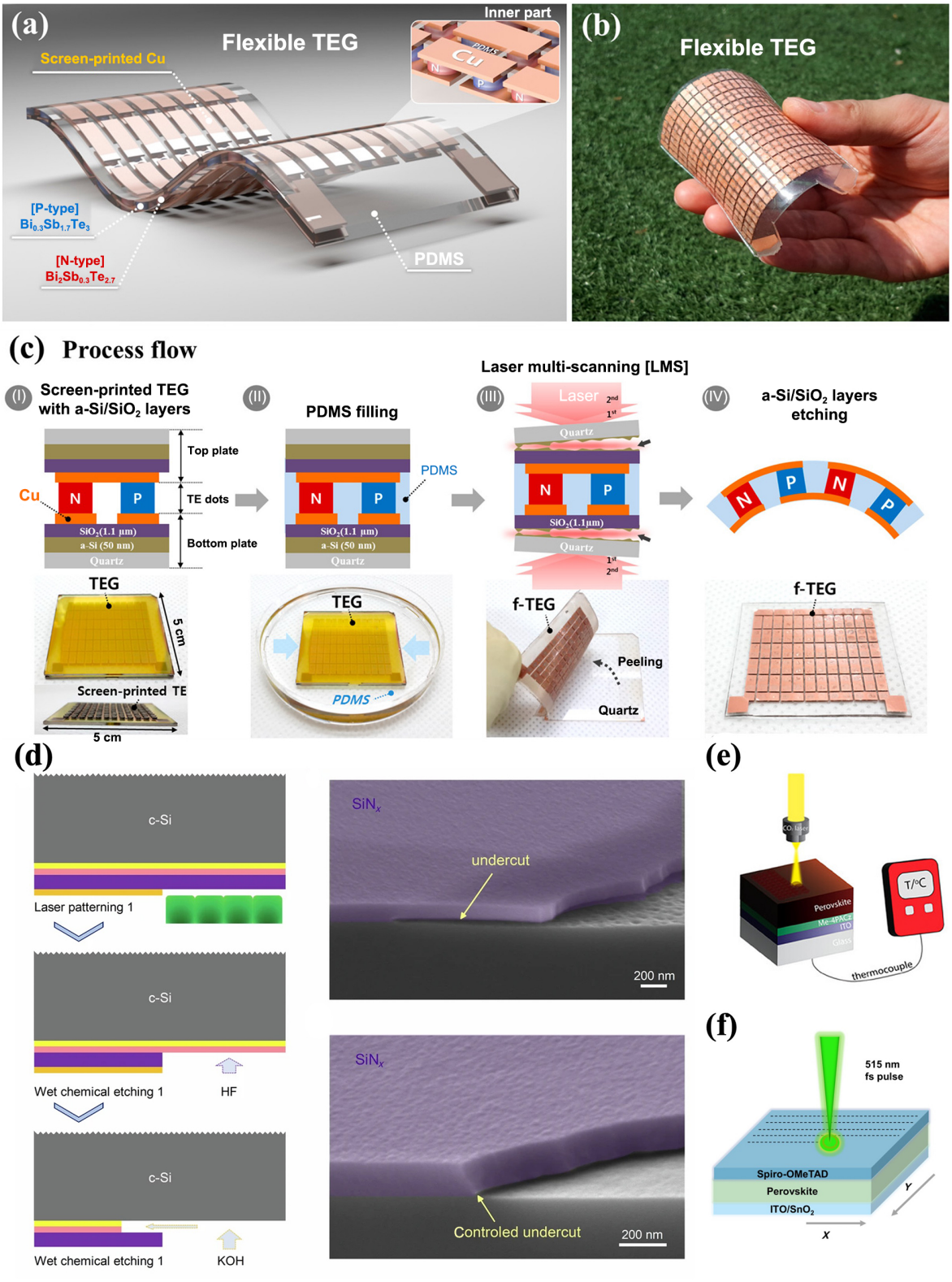

Figure 9 (a) and (b) Schematic illustration and corresponding photograph of the freestanding f-TEG prepared using a LMS lift-off process. (c) Fabrication steps of a freestanding f-TEG. (I) Preparation of the screen-printed TEG with top and bottom substrates (SiO_2/amorphous Si (a-Si)/quartz plate). (II) Infiltrating the elastic polymer (PDMS) into the gap between the TE legs. (III) Removal of the top and bottom plates using the LMS process. (IV) Removing the remaining SiO_2/a-Si layers by etching in a diluted mixture of hydrogen fluoride and hydrochloric acid. Reproduced with permission from Ref. [152], © American Chemical Society 2016. (d) Illustration of the laser patterning 1 and wet chemical cleaning process for undercut formation. Reproduced with permission from Ref. [154], © Wu, H. et al., under exclusive licence to Springer Nature Limited 2024. (e) Schematic of experimental temperature measurement setup using thermocouple attached to the center of the glass substrate rear. Reproduced with permission from Ref. [155], © Yi, J. P. et al. 2025. (f) Schematic diagram of ultrafast laser irradiation processing. Reproduced with permission from Ref. [156], © Meng, J. Q. et al. 2024.

(CIGS) thin films and systematically studied the effects of FS-LA treatment on the structure and photoelectrical property of CIGS thin films. It has been demonstrated that femtosecond laser annealing of CIGS films printed via a non-vacuum ink process can markedly enhance the crystalline quality and suppress film defects without inducing melting. Experimental results suggest that FS-LA provides a reliable means to improve the photovoltaic conversion efficiency of flexible, ink-printed CIGS thin films. Wilkes et al. [161] introduced a novel laser annealing process. They validated the structure and composition of laser-annealed TiO_2 and demonstrated its properties through four-point probe measurements and illumination current–voltage scanning. It is shown that the reactions of membrane hydrolysis, condensation, water removal, hydroxyl removal, and Ti–O–Ti bond occur within tens of nanoseconds, which is equivalent to the width of a laser pulse. The efficiency of laser-processing solar cells surpasses that of counterparts fabricated via conventional hot-plate methods. Tai et al. [162] used a laser-induced ultrafast single-source evaporation employing a CNT evaporator to prepare high-quality methylammonium lead iodide perovskite films, which were subsequently utilized to construct high-performance solar cells. Planar solar cells using these perovskite films (0.06 cm^2) showed an optimal power conversion efficiency of 16.8% with no significant hysteresis, one of the highest power conversion efficiencies using the gas-based deposition method. Hadi et al. [163] fabricated a dense mesoporous titanium dioxide layer using a single-step laser irradiation technique, followed by preparing high-performance dye-sensitized solar cells (DSSCs). With the laser process, the overall manufacturing time of DSSCs was significantly reduced from 5 h and 20 min to 2 min. The maximum power conversion efficiency of laser-processed DSSCs is 34% higher than that of their heating-furnace-processed counterparts. Belchi et al. [164] proposed a method for synthesizing TiO_2/graphene nanocomposites using laser pyrolysis to improve perovskite solar cells. The results showed that the power conversion efficiency of the TiO_2 electrode is significantly improved under standard light, with an average efficiency of 15.3%, while that of the pure TiO_2 electrode is 13.8%.

4.3 Laser-processed electrodes in sensor applications

4.3.1 Biosensors

Electrodes play a pivotal role in modern sensor technologies, encompassing biosensors for the detection of glucose, neurotransmitters, uric acid, tyrosine, lactic acid, and other biomolecules, as well as chemical sensors for monitoring ion concentrations of natural waters, non-electrolytic detection of trace phenol contaminants, and pH measurement in beverages. Cao et al. [165] were the first to use LDW-based nano-3D printing to fabricate implantable carbon nanoelectrodes for dopamine sensing. The biosensor successfully detected dopamine in the brains of adult fruit flies. The fabrication method enables precise control and high reproducibility of the carbon nanoelectrodes, offering excellent potential for flexible design of carbon-nanoelectrode architectures for diverse applications. Yang et al. [166] developed an all-laser-sculpted sweat sensor capable of continuously monitoring temperature, respiratory rate, and trace concentrations of uric acid and tyrosine, thereby enabling real-time analysis of biomarkers associated with gout and metabolic disorders, as shown in Fig. 10(a). The sensor consists of a highly sensitive laser-engraved graphene-based chemical sensor (LEG-CS) for monitoring low concentrations of uric acid and tyrosine, a LEG-based physical sensor (LEG-PS) for monitoring temperature and respiration rate, and a laser-sculpted multi-entry microfluidic module for dynamic sweat sampling. Glucose, the primary energy source for living organisms, plays an essential role in metabolism. Accurate monitoring of blood glucose is particularly crucial for patients with diabetes; hence, there is an urgent need for simple, rapid, and cost-effective glucose sensors.

Khairullina et al. [10] fabricated a glucose sensor using the laser-induced selective surface activation method. The sensor has a sensitivity of 3060 $\mu A \cdot mM^{-1} \cdot cm^{-2}$ for glucose sensing and a linear range from 0.3 to 1000 μM for glucose detection, showing high selectivity and long-term stability. Meng et al. [167] developed a flexible skin-patch biosensor based on LIG capable of simultaneously detecting lactic acid and glucose. The conductive-polymer modification of LIG significantly enhanced its contact stability and electrochemical performance, demonstrating considerable potential for wearable biochemical sensing. Lei et al. [168] used a laser-engraving process to transform lignin precursors into nitrogen-doped graphene patterns and to prepare biochemical sensors for detecting glucose, lactic acid, and alcohol. They introduced two-dimensional MXene ($Ti_3C_2T_x$) nanosheets into the N-LSG electrode and synthesized MXene/Prussian blue ($Ti_3C_2T_x$/PB) composites for the detection of hydrogen peroxide. Finally, the electrode was functionalized using different catalytic enzymes. Gao et al. [169] fabricated a high-performance glucose sensor by LDW technology, with a sensitivity of 13.822 $mA \cdot cm^{-2} \cdot mM^{-1}$ and a detection limit of 1.9×10^{-6} M. The integration of a super-hydrophilic nickel foam further enhanced the device's electrochemical activity and overall sensing performance.

4.3.2 Chemical sensors

Xu et al. [131] reported an LSG-based electrochemical sensor exhibiting high selectivity for DA detection even in the presence of ascorbic acid (AA) and uric acid (UA). In parallel, Cheng et al. [170] prepared a high-performance bisphenol A (BPA) sensor using LDW, which enables on-site detection of trace BPA concentrations of river water. Song et al. [171] prepared a paper solid electrochemical sensor for on-site detection of trace phenol pollutants in non-electrolysis water by laser cutting (Fig. 10(b)). Lonsdale et al. [172] prepared a sensor that could accurately measure the pH of beer based on RuO_2 deposited by laser etch sputtering on an Al_2O_3 substrate. Laser processing has also enabled improved sensing architectures. Yan et al. [173] optimized the morphology of an MoS_2 gas sensor using a laser-induced graphene electrode, while Beduk et al. [174] used LSG combined with a 3D gold nanostructure to develop a smart antibody sensor for COVID-19 diagnosis. Yu et al. [175] fabricated a flexible sensor array electronic tongue system to detect salty, sweet, and sour tastes using LDW technology.

A central theme is that femtosecond, picosecond, or CO_2 laser irradiation can directly convert polymeric or photoresist precursors into a porous, electronically conductive, graphene-like network (LIG) while simultaneously defining the electrode geometry. This *in situ* laser writing step avoids lithography and metal lift-off, lowers thermal budget, and preserves mechanical compliance, making it attractive for epidermal and flexible sensing. Lim et al. [176] showed that ultraviolet-laser-induced graphene can act as both a mechanically robust current collector and a templated growth scaffold for a semiconducting MOF film (Cu_3HHTP_2), yielding an NO_2 gas sensor with sub-ppb detection limits, sub-20 s

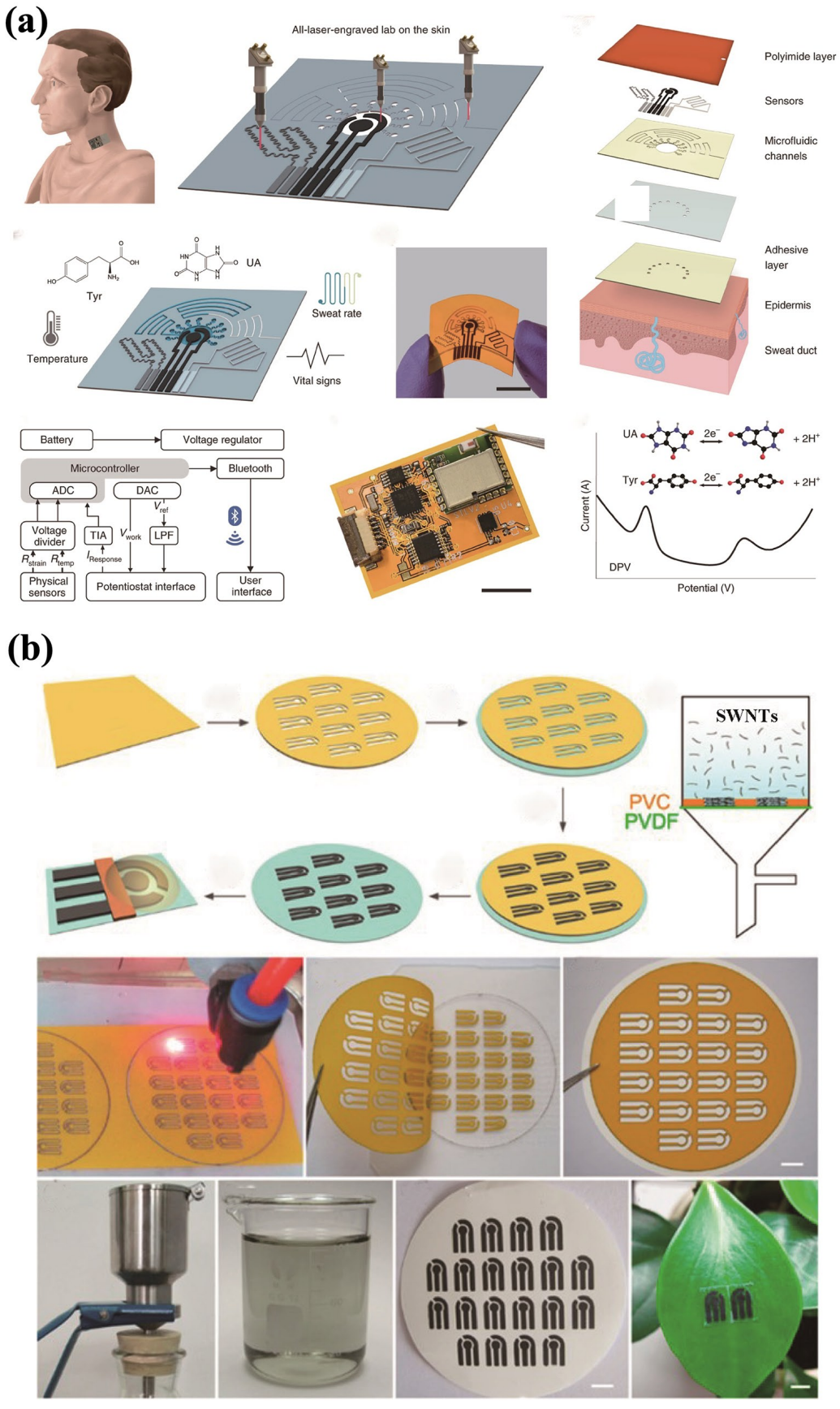

Figure 10 (a) Schematics of the sweat sensor for metabolic and nutritional management. Reproduced with permission from Ref. [166], © Yang, Y. R. et al., under exclusive licence to Springer Nature America, Inc. 2020. (b) Schematics of carbon-nanomaterial-based electrochemical sensors. Reproduced with permission from Ref. [171], © American Chemical Society 2018.

response/recovery at room temperature, and mechanical flexibility. The hierarchical pore architecture that emerges at the laser-written carbon/MOF interface accelerates mass transport and charge transfer, demonstrating that laser processing can "place" high-surface-area, redox-active sensing phases exactly where they are needed while preserving bendability and enabling wearable air-quality monitoring.

5 Challenges and opportunities

5.1 Critical challenges

5.1.1 Dimension- and scenario-dependent reliability under cycling

Ensuring the long-term reliability of laser-fabricated micro/nano electrodes remains a primary barrier to practical deployment because degradation pathways depend strongly on dimensional architecture (1D/2D/3D) and application scenario (textile/flexible chips/monolithic micro-power), discussed in Sections 3 and 4. Even for devices intended to operate in static environments, residual stress from fabrication, thermal expansion mismatch, and handling can trigger damage accumulation over time [177].

For 1D electrode (fibers/lines/yarns), reliability is frequently dominated by junction integrity and fatigue under repeated bending/torsion, particularly for welded nanowire or filamentary networks. Junction degradation can manifest as contact resistance drift, interconnect discontinuity, and loss of percolation under cyclic strain. For wearable and strain-bearing platforms, durability enhancement strategies from flexible electronics (e.g., strain-distribution design, encapsulation, and mechanical neutral-plane engineering) should be explicitly considered in electrode design and packaging [177].

Planar microelectrodes are vulnerable to crack initiation at patterned edges, delamination, and electrochemically accelerated damage under repeated flexing. Beyond pure mechanical cracking, "electromechanical degradation" (mechanical deformation and electrochemical reactions) has been emphasized as an under-characterized failure mode, largely because standardized protocols for combined mechanical–electrochemical testing are still limited [178]. This challenge is particularly relevant to flexible MSCs and on-skin systems, where repeated bending and environmental exposure (humidity/sweat) can accelerate interface degradation [177,179].

3D architectures have improved transport and high mass loading, but introduce reliability risks including microcracking, interlayer debonding, and stress concentration in high-aspect-ratio structures. Additionally, 3D electrodes often rely on electrolyte infiltration and stable interfaces, and incomplete wetting or local depletion can lead to non-uniform utilization and premature failure. Practical reliability assessment should thus include structure-sensitive tests (e.g., *in situ* impedance under mechanical cycling, electrolyte infiltration stability, and thermal shock tests) in addition to standard galvanostatic cycling [178].

Across all dimensions, improving reliability requires (i) standardized durability protocols (mechanical + electrochemical combined), (ii) accelerated aging tests (thousands of bending/thermal cycles), and (iii) *in situ*/*operando* diagnostics (e.g., resistance mapping, EIS during deformation, and microscopy for crack evolution). These measures will enable meaningful comparisons among laser-processed electrodes and support the reliability demanded by heterointegrated devices.

5.1.2 Process compatibility and cross-platform integration

A second major challenge is ensuring that laser-fabricated electrodes and their process windows are compatible with heterogeneous substrates and integration strategies. Electrode architectures for rigid substrates (Si/glass) may not directly translate to flexible/stretchable platforms because the mechanical compliance requirements differ substantially [179].

Rigid systems tolerate high-aspect-ratio features and thick films, whereas flexible systems require bending tolerance, and stretchable systems require large strain accommodation. Stretchable electronics commonly use serpentine/meandering/fractal layouts to distribute strain and protect functional regions [180, 181]. However, these strain-engineering approaches can be area-inefficient or unnecessary for rigid integration, making cross-platform transfer nontrivial.

Many polymer substrates (PET/TPU/PI) have limited thermal budgets; therefore, process compatibility depends on controlling heat-affected zones, debris redeposition, and surface chemistry changes induced by laser processing. Substrate selection and packaging constraints (solvent resistance, temperature limits, optical transparency) further define viable process windows [179].

For soft bioelectronics and organoid interfaces, compatibility extends to biocompatibility, long-term stability in biofluids, and gentle mechanical coupling with tissue [182]. In such scenarios, laser microfabrication can be attractive for patterned micro/nanotopographies, but the electrode and encapsulation should prevent biofouling and maintain stable impedance.

Overall, improved cross-platform compatibility requires dimension-specific design rules (Sections 3 and 4) to be formalized into platform-aware process guidelines, including substrate-dependent parameter windows, packaging choices, and geometry libraries for rigid/flexible/stretchable implementations.

5.1.3 Practical implementation: scalability, reproducibility, and standardization

Even when performance is promising at the lab scale, practical implementation is often limited by scalability, reproducibility, and quality control. Laser processing is inherently attractive for maskless, programmable manufacturing, but the translation to practical implementation requires: (i) scalability and throughput: many laser routes are serial (scanning-based), and throughput depends on scan strategy, spot size, and multi-beam parallelization. For high-volume production, parameter robustness and process monitoring become critical; (ii) reproducibility and quality control: performance variability can arise from precursor variability (inks/films), substrate nonuniformity, debris accumulation, and environment-dependent chemistry. Standardized reporting (laser parameters, feature sizes, and test conditions) and statistical yield metrics are necessary to compare methods across studies and to enable technology transfer; (iii) integration and packaging: in practical implementation, electrolyte containment, encapsulation, and electrical interconnects should be considered. In particular, flexible and wearable devices require mechanically compliant packaging that does not compromise ionic access or induce delamination [165, 167].

5.2 Emerging opportunities

5.2.1 Materials and structural innovations guided by architecture

Rapid progress in materials science is opening opportunities to

enhance laser-fabricated electrodes through novel materials and hierarchical structures. One promising direction is the development of hierarchical hybrid electrodes that combine multiple materials or length-scale structures to synergistically improve performance. Integrating nanostructures into micro- to macroscale frameworks enables these hybrids to simultaneously achieve large surface area, enhanced electrical conductivity, and robust mechanical integrity. Likewise, MXene (2D transition metal carbides/nitrides) has emerged as an attractive electrode owing to its metallic conductivity and rich surface chemistry. MXene-based flexible electrodes are being widely explored for MSCs and MBs. Numerous studies have demonstrated that MXene films can achieve excellent gravimetric and volumetric capacitance, but they often suffer from restacking of the atomic layers, which reduces accessible surface area and ion transport. To overcome this, flexible MXene hybrids and composites are designed. For instance, spacers (nanoparticles, polymers, or 1D/2D fillers) are introduced to prevent layer collapse and preserve porosity. Such strategies yielded composite films with high electrical conductivity and improved capacity retention by mitigating self-stacking effects. By leveraging hierarchical structures (e.g., porous networks and layered composites), future laser-fabricated electrodes will achieve higher energy density, faster response, and greater durability than conventional single-material planar designs.

5.2.2 Multifunctional integration for advanced devices

Laser-fabricated micro/nano electrodes hold great promise for enabling multifunctional device integration, whereby a single electrode or electrode network can serve multiple roles in energy storage, energy harvesting, sensing, and actuation within a heterointegrated device.

One exciting opportunity is the fusion of energy storage and sensing functionalities. Instead of treating power units (MBs/MSCs) and sensors as separate components, researchers are developing electrode architectures that can simultaneously store energy and monitor environmental or physiological signals. For example, a recent study demonstrated a flexible film electrode (V_2O_5/MXene composite) that functions as both a Zn-ion MB cathode and a strain/pressure sensor in a wearable device [183]. This self-powered sensor concept enables the energy device to provide real-time sensing without an external power source. Similarly, interdigital MSC electrodes based on MXene/TiS_2 are integrated with ionic sensors, creating a single platform that functions as an energy reservoir and a responsive pressure sensor [184]. These approaches illustrate how laser-fabricated electrodes with finely designed geometry and composition can achieve dual-use functionality, improving device compactness and efficiency.

Beyond energy-sensing combination, there is significant interest in using laser microfabrication for soft bioelectronics and neural interfaces. Heterointegrated biomedical devices, such as brain–machine interfaces or wearable health monitors, place stringent requirements on electrodes that exhibit high electrical efficiency, mechanical compliance, and biocompatibility. Laser processing offers the precision to create micro/nanostructured electrodes (e.g., microneedle arrays or textured neural probes) that can interface gently with neural or epidermal tissue [182]. The opportunity here is to leverage laser micromachining to produce bio-integrated electrodes that combine sensing/stimulation capabilities with therapeutic or energy functionalities (such as a neural probe that also delivers localized electrical stimulation powered by an MSC).

In summary, multifunctional integration enabled by laser-fabricated electrodes could lead to self-sustaining wearable devices, closed-loop sensor-actuator devices, and advanced implantable devices—all with reduced size and improved component synergy.

5.2.3 Machine learning and data-driven materials/process design

A major frontier opportunity is to adopt data-driven workflows to accelerate "process–structure–performance" optimization. For supercapacitor materials, machine-learning approaches have been used to identify critical features (e.g., pore structure and heteroatom content) and guide synthesis strategies. For example, machine-learning-assisted design was reported to guide the development of highly porous carbon materials (specific surface area > 4000 $m^2 \cdot g^{-1}$) and high specific capacitance (~ 610 $F \cdot g^{-1}$ in 1M H_2SO_4), illustrating how data-driven strategies can reduce trial-and-error in materials discovery [185].

For laser processing, Bayesian optimization has been demonstrated as a sample-efficient approach for optimizing laser cutting, welding, and polishing with modest expert input, suggesting a practical pathway to optimize laser parameter windows for micro/nano electrodes while minimizing experimental cost. Beyond offline optimization, future work can integrate in-line metrology (optical/thermal/electrical signals) with ML models to predict feature formation, detect defects, and enable adaptive control for yield and uniformity.

5.2.4 Multiphysics simulation and computational modeling for mechanism-to-manufacturing translation

Laser fabrication inherently involves coupled mechanisms (heat transfer, phase transitions, fluid flow, stress evolution, and sometimes electrochemistry). Multiphysics modeling can provide mechanistic insight and guide parameter selection prior to large-scale experimental campaigns. Recent work demonstrates multiphysics simulations that explicitly couple temperature, electric, and flow fields to predict structure formation and validate against experiments, highlighting the value of multiphysics approaches for understanding and controlling complex laser-enabled micromachining processes [186].

In parallel, physics-informed machine learning is emerging as a promising approach to real-time prediction and control in welding and additive manufacturing by combining governing equations with sparse data. For micro/nano electrodes, such approaches could enable "digital twins" that link laser parameters to the expected microstructure (porosity, junction quality, and channel geometry), and ultimately, to electrochemical performance, thereby improving reproducibility and accelerating scaling.

6 Conclusion

The rapid proliferation of smart, interconnected electronic systems has intensified demand for high-efficiency, miniaturized energy storage technologies across platforms ranging from wearable electronics to implantable biomedical devices and electric vehicles. This review presents several fabrication strategies for micro/nanoscale energy devices that are specifically processed by laser-involved techniques. Based on the physical–chemistry nature of the processing methods, these techniques can be broadly divided into two categories: physical modification processes, including laser

etching, cutting, marking, and deposition, and chemical transformations, represented by laser-induced reactions and laser carbonization.

Laser processing offers distinct advantages for micro/nanoscale processing. Micro/nanoscale energy devices can be designed to meet specific structural requirements and allow for refined control within the laser HAZ during fabrication. In this review, energy devices are categorized by dimensionality, revealing that higher-dimensional architectures demand more advanced processing technologies. The development of 1D/2D/3D laser-processed micro/nano electrodes not only enhances the overall performance of the device but also imposes greater demands on fabrication precision and processing technology. In most cases, laser-based 3D printing is employed to construct such intricate architectures. Furthermore, this review summarizes the applications of these energy devices across three domains: energy storage, energy supply, and energy conversion. Clearly, the application of energy devices is extensive and has broad prospects for development. In addition, various new materials, such as MXenes and graphene, have been applied in energy storage devices.

Advances in laser processing and emerging materials have significantly enhanced the miniaturization and flexibility of energy storage devices. However, energy storage devices still face significant challenges. First, the most important thing is to increase the energy density. Continued advances in surface modification, structural design, and material selection are expected to drive improvements in energy density. Achieving high-energy-density storage is vital for prolonging the operational lifetime of implantable and other invasive electronic devices. Furthermore, the pursuit of low-cost, high-throughput fabrication of micro/nanoscale energy devices, together with enhanced safety and environmental sustainability, will remain central themes in the future development of energy technologies.

Acknowledgements

This work was financially supported by the Fundamental Research Funds for the Central Universities of China (Nos. 2024JCG001 and 20822041F4045), the National Natural Science Foundation of China (No. 52373249), and the Science and Technology Project of Yibin Sanjiang New Area (No. 2023SJXQSXZJ003).

Declaration of competing interest

All the contributing authors report no conflict of interests in this work.

Author contribution statement

Y. H. L.: Data curation, investigation, validation, visualization, writing manuscript. Y. F. S.: Validation, visualization, writing manuscript. L. H.: Funding acquisition, visualization, writing manuscript. R. Q. S.: Investigation, writing manuscript. J. Y. Z.: Investigation, writing manuscript. X. M. Y.: Investigation, writing manuscript. Z. P.: Visualization, writing manuscript. Z. Y. M.: Investigation, writing manuscript. W. W. W.: Investigation, writing manuscript. J. B. C.: Visualization, writing manuscript. Y. X. D.: Visualization, writing manuscript. S. Y. Y.: Funding acquisition, writing manuscript. D. L.: Validation, visualization, writing manuscript. H. B. Y.: Validation, visualization, writing manuscript. P. T.: Formal analysis, supervision, visualization, writing manuscript.

Use of AI statement

None.

References

[1] Yoo, H.; Mahato, M.; Oh, W.; Ha, J.; Han, H. E.; Ahn, C. W.; Oh, I. K. Exploring role of microbatteries in enhancing sustainability and functionality of implantable biosensors and bioelectronics. *Biosens. Bioelectron.* **2024**, *260*, 116419.

[2] Yu, L. H.; Li, W. P.; Wei, C. H.; Yang, Q. F.; Shao, Y. L.; Sun, J. Y. 3D printing of NiCoP/Ti_3C_2 MXene architectures for energy storage devices with high areal and volumetric energy density. *Nano-Micro Lett.* **2020**, *12*, 143.

[3] Huang, L. B.; Su, J. J.; Song, Y.; Ye, R. Q. Laser-induced graphene: En route to smart sensing. *Nano-Micro Lett.* **2020**, *12*, 157.

[4] Lin, J.; Peng, Z. W.; Liu, Y. Y.; Ruiz-Zepeda, F.; Ye, R. Q.; Samuel, E. L. G.; Yacaman, M. J.; Yakobson, B. I.; Tour, J. M. Laser-induced porous graphene films from commercial polymers. *Nat. Commun.* **2014**, *5*, 5714.

[5] Kumar, N.; Sahoo, P. K.; Lee, S. Y.; Park, S. J. Recent laser advances in graphene-based planar micro-supercapacitors: Challenges and future prospects. *Sustainable Mater. Technol.* **2024**, *40*, e00962.

[6] Li, H. P.; Luo, J. H.; Ding, S. M.; Ding, J. B. Laser-machined micro-supercapacitors: From microstructure engineering to smart integrated systems. *Nanoscale* **2024**, *16*, 14574–14588.

[7] Peng, Y. Y.; Akuzum, B.; Kurra, N.; Zhao, M. Q.; Alhabeb, M.; Anasori, B.; Kumbur, E. C.; Alshareef, H. N.; Ger, M. D.; Gogotsi, Y. All-MXene (2D titanium carbide) solid-state microsupercapacitors for on-chip energy storage. *Energy Environ. Sci.* **2016**, *9*, 2847–2854.

[8] Ikram, M.; Salunke, P.; Numan, A.; Sher, M. Development, fabrication, and applications of laser-induced graphene-based biosensors in food and dairy sectors. *Microchim. Acta* **2025**, *192*, 554.

[9] Wang, S. G.; Tan, C. J.; Zong, Q. H.; Li, S. Z.; Gao, C. S.; Yang, H. R.; Huang, Q. M.; French, P.; Ye, H. Y. Selective reduction laser sintering: A new strategy for NO_2 gas detection based on In_2O_3 nanoparticles. *Adv. Funct. Mater.* **2025**, *35*, 2419057.

[10] Khairullina, E. M.; Panov, M. S.; Andriianov, V. S.; Ratautas, K.; Tumkin, I. I.; Račiukaitis, G. High rate fabrication of copper and copper-gold electrodes by laser-induced selective electroless plating for enzyme-free glucose sensing. *RSC Adv.* **2021**, *11*, 19521–19530.

[11] Ji, Y. Q.; Liao, Y. X.; Li, H. H.; Cai, Y. H.; Fan, D. L.; Liu, Q.; Huang, S. B.; Zhu, R. J.; Wang, S.; Wang, H. Q. et al. Flexible metal electrodes by femtosecond laser-activated deposition for human–machine interfaces. *ACS Appl. Mater. Interfaces* **2022**, *14*, 11971–11980.

[12] Parmeggiani, M.; Zaccagnini, P.; Stassi, S.; Fontana, M.; Bianco, S.; Nicosia, C.; Pirri, C. F.; Lamberti, A. PDMS/polyimide composite as an elastomeric substrate for multifunctional laser-induced graphene electrodes. *ACS Appl. Mater. Interfaces* **2019**, *11*, 33221–33230.

[13] Zhang, W. L.; Lei, Y. J.; Jiang, Q.; Ming, F. W.; Costa, P. M. F. J.; Alshareef, H. N. 3D laser scribed graphene derived from carbon nanospheres: An ultrahigh-power electrode for supercapacitors. *Small Methods* **2019**, *3*, 1900005.

[14] Esqueda-Barrón, Y.; Pérez del Pino, A.; Lebière, P. G.; Musheghyan-Avetisyan, A.; Bertran-Serra, E.; György, E.; Logofatu, C. Boost of charge storage performance of graphene nanowall electrodes by laser-induced crystallization of metal oxide nanostructures. *ACS Appl. Mater. Interfaces* **2021**, *13*, 17957–17970.

[15] Kang, S. M.; Lim, K.; Park, H.; Park, J. B.; Park, S. C.; Cho, S. P.; Kang, K.; Hong, B. H. Roll-to-roll laser-printed graphene-graphitic carbon electrodes for high-performance supercapacitors. *ACS Appl. Mater. Interfaces* **2018**, *10*, 1033–1038.

[16] Nie, B. B.; Li, X. M.; Shao, J. Y.; Li, C. M.; Sun, P. C.; Wang, Y. C.; Tian, H. M.; Wang, C. H.; Chen, X. L. Scalable fabrication of high-performance micro-supercapacitors by embedding thick interdigital microelectrodes into microcavities. *Nanoscale* **2019**, *11*, 19772–19782.

[17] Singh, S. P.; Li, Y. L.; Be'er, A.; Oren, Y.; Tour, J. M.; Arnusch, C. J. Laser-induced graphene layers and electrodes prevents microbial fouling and exerts antimicrobial action. *ACS Appl. Mater. Interfaces* **2017**, *9*, 18238–18247.

[18] Zhou, W. P.; Bai, S.; Ma, Y.; Ma, D. L.; Hou, T. X.; Shi, X. M.; Hu, A. M. Laser-direct writing of silver metal electrodes on transparent flexible substrates with high-bonding strength. *ACS Appl. Mater. Interfaces* **2016**, *8*, 24887–24892.

[19] Zhu, Z. Z. An overview of carbon nanotubes and graphene for biosensing applications. *Nano-Micro Lett.* **2017**, *9*, 25.

[20] Getachew, B. A.; Bergsman, D. S.; Grossman, J. C. Laser-induced graphene from polyimide and polyethersulfone precursors as a sensing electrode in anodic stripping voltammetry. *ACS Appl. Mater. Interfaces* **2020**, *12*, 48511–48517.

[21] Paula, K. T.; Lin, H. I.; Yang, F.; Vollet-Filho, J. D.; Gu, T.; Hu, J.; Mendonça, C. R. Femtosecond laser processing of amorphous silicon films. *J. Manuf. Processes* **2024**, *128*, 50–59.

[22] Peng, H.; Kopic, I.; Potfode, S. R.; Teshima, T. F.; Boustani, G. A.; Hiendlmeier, L.; Wang, C.; Hussain, M. Z.; Özkale, B.; Fischer, R. A. et al. Laser-patterned epoxy-based 3D microelectrode arrays for extracellular recording. *Nanoscale* **2024**, *16*, 14295–14301.

[23] Yuan, Y. F.; Zuo, P.; Li, F.; Wang, G. Y.; Zhang, K. H.; Tian, H.; Han, W. N.; Rao, H. R.; Lv, L.; Huo, Y. Z. et al. Advances in laser processing technologies for 2D materials and perovskite-based flexible electronics. *Adv. Eng. Mater.* **2025**, *27*, 2501441.

[24] Rox, H.; Ränke, F.; Mädler, J.; Marzec, M. M.; Sokołowski, K.; Baumann, R.; Hamedi, H.; Yang, X. G.; Mutschke, G.; Urbas, L. et al. Boosting electrode performance and bubble management via direct laser interference patterning. *ACS Appl. Mater. Interfaces* **2025**, *17*, 9364–9377.

[25] Liu, X.; Liu, Q. L.; Luo, M. D.; Xu, L.; Kuang, C. F.; Liu, X. Super-resolution direct laser writing via multiphoton and peripheral photoinhibition photolithography. *Opt. Lett.* **2025**, *50*, 1675–1678.

[26] Zhang, X.; Wang, C. S.; Yang, W. F.; Gao, D. D.; Zhang, Z. Y.; Dong, X. L. Laser-sintering fabrication of integrated Al/Ni anodes for lithium-ion batteries. *RSC Adv.* **2022**, *12*, 13168–13179.

[27] Wu, H.; Fahy, W. P.; Kim, S.; Kim, H.; Zhao, N.; Pilato, L.; Kafi, A.; Bateman, S.; Koo, J. H. Recent developments in polymers/polymer nanocomposites for additive manufacturing. *Prog. Mater. Sci.* **2020**, *111*, 100638.

[28] Awad, A.; Fina, F.; Goyanes, A.; Gaisford, S.; Basit, A. W. 3D printing: Principles and pharmaceutical applications of selective laser sintering. *Int. J. Pharm.* **2020**, *586*, 119594.

[29] Yan, L.; Chen, Y. T.; Liou, F. Additive manufacturing of functionally graded metallic materials using laser metal deposition. *Addit. Manuf.* **2020**, *31*, 100901.

[30] Ramos, E.; Browar, A.; Roehling, J.; Ye, J. C. CO_2 laser sintering of garnet-type solid-state electrolytes. *ACS Energy Lett.* **2022**, *7*, 3392–3400.

[31] Huang, H. C.; Chu, X.; Xie, Y. T.; Zhang, B. B.; Wang, Z. X.; Duan, Z. Y.; Chen, N. J.; Xu, Z.; Zhang, H. T.; Yang, W. Q. $Ti_3C_2T_x$ MXene-based micro-supercapacitors with ultrahigh volumetric energy density for all-in-one Si-electronics. *ACS Nano* **2022**, *16*, 3776–3784.

[32] Chen, K. Y.; Gao, C.; Lu, B.; Jin, X. T.; Shao, C. X.; Wang, J. Q.; Wu, W. P.; Qu, L. T.; Zhao, Y. A facile laser assisted paste-tear approach to large area, flexible and wearable in-plane micro-supercapacitors. *J. Power Sources* **2022**, *532*, 231346.

[33] Yu, W. J.; Zhao, W. W.; Liu, X. Q. Pulsed laser welding of macroscopic 3D graphene materials. *Mater. Horiz.* **2023**, *10*, 5597–5606.

[34] Dunlap, N.; Sulas-Kern, D. B.; Weddle, P. J.; Usseglio-Viretta, F.; Walker, P.; Todd, P.; Boone, D.; Colclasure, A. M.; Smith, K.; Tremolet de Villers, B. J.; Finegan, D. P. Laser ablation for structuring Li-ion electrodes for fast charging and its impact on material properties, rate capability, Li plating, and wetting. *J. Power Sources* **2022**, *537*, 231464.

[35] Liang, C.; Sun, X. Y.; Su, W. M.; Hu, Y. W.; Duan, J. Fast welding of silver nanowires for flexible transparent conductive film by spatial light modulated femtosecond laser. *Adv. Eng. Mater.* **2021**, *23*, 2100584.

[36] Chen, W.; Liu, L. X.; Zhang, H. B.; Yu, Z. Z. Flexible, transparent, and conductive $Ti_3C_2T_x$ MXene-silver nanowire films with smart acoustic sensitivity for high-performance electromagnetic interference shielding. *ACS Nano* **2020**, *14*, 16643–16653.

[37] Gao, W.; Singh, N.; Song, L.; Liu, Z.; Reddy, A. L. M.; Ci, L.; Vajtai, R.; Zhang, Q.; Wei, B. Q.; Ajayan, P. M. Direct laser writing of micro-supercapacitors on hydrated graphite oxide films. *Nat. Nanotechnol.* **2011**, *6*, 496–500.

[38] Lee, S. M.; Park, Y. J.; Kim, J. H. Laser reduction of Zn-infiltrated multilayered graphene oxide as electrode materials for supercapacitors. *ACS Appl. Nano Mater.* **2019**, *2*, 3711–3717.

[39] Xu, G. Y.; Jarjes, Z. A.; Wang, H. W.; Phillips, A. R. J.; Kilmartin, P. A.; Travas-Sejdic, J. Detection of neurotransmitters by three-dimensional laser-scribed graphene grass electrodes. *ACS Appl. Mater. Interfaces* **2018**, *10*, 42136–42145.

[40] Fu, X. Y.; Chen, D. L.; Liu, Y.; Jiang, H. B.; Xia, H.; Ding, H.; Zhang, Y. L. Laser reduction of nitrogen-rich carbon nanoparticles@graphene oxides composites for high rate performance supercapacitors. *ACS Appl. Nano Mater.* **2018**, *1*, 777–784.

[41] Zhu, J. B.; Huang, X.; Song, W. X. Physical and chemical sensors on the basis of laser-induced graphene: Mechanisms, applications, and perspectives. *ACS Nano* **2021**, *15*, 18708–18741.

[42] Vivaldi, F. M.; Dallinger, A.; Bonini, A.; Poma, N.; Sembranti, L.; Biagini, D.; Salvo, P.; Greco, F.; Di Francesco, F. Three-Dimensional (3D) laser-induced graphene: Structure, properties, and application to chemical sensing. *ACS Appl. Mater. Interfaces* **2021**, *13*, 30245–30260.

[43] Fenzl, C.; Nayak, P.; Hirsch, T.; Wolfbeis, O. S.; Alshareef, H. N.; Baeumner, A. J. Laser-scribed graphene electrodes for aptamer-based biosensing. *ACS Sens.* **2017**, *2*, 616–620.

[44] Alhajji, E.; Wang, W. X.; Zhang, W. L.; Alshareef, H. N. A hierarchical three-dimensional porous laser-scribed graphene film for suppressing polysulfide shuttling in lithium-sulfur batteries. *ACS Appl. Mater. Interfaces* **2020**, *12*, 18833–18839.

[45] Zhang, Z. H.; Yang, W. M.; Cheng, L. S.; Cao, W. Y.; Sain, M.; Tan, J.; Wang, A.; Jia, H. B. Carbon fibers with high electrical conductivity: Laser irradiation of mesophase pitch filaments obtains high graphitization degree. *ACS Sustainable Chem. Eng.* **2020**, *8*, 17629–17638.

[46] Lazauskas, A.; Marcinauskas, L.; Andrulevicius, M. Modification of graphene oxide/$V_2O_5{\cdot}nH_2O$ nanocomposite films via direct laser irradiation. *ACS Appl. Mater. Interfaces* **2020**, *12*, 18877–18884.

[47] Yu, Y. C.; Chen, M.; Wang, S. T.; Hill, C.; Joshi, P.; Kuruganti, T.; Hu, A. M. Laser sintering of printed anodes for Al-air batteries. *J. Electrochem. Soc.* **2018**, *165*, A584–A592.

[48] Zhu, P. H.; Sterzl, Y.; Pfleging, W. Impact of laser ablation strategies

on electrochemical performances of 3D batteries containing aqueous acid processed $Li(Ni_{0.6}Mn_{0.2}Co_{0.2})O_2$ cathodes with high mass loading. *Batteries* **2024**, *10*, 354.

[49] Jiao, S. Q.; Zhou, A. G.; Wu, M. Z.; Hu, H. B. Kirigami patterning of MXene/bacterial cellulose composite paper for all-solid-state stretchable micro-supercapacitor arrays. *Adv. Sci.* **2019**, *6*, 1900529.

[50] Garnett, E. C.; Cai, W. S.; Cha, J. J.; Mahmood, F.; Connor, S. T.; Greyson Christoforo, M.; Cui, Y.; McGehee, M. D.; Brongersma, M. L. Self-limited plasmonic welding of silver nanowire junctions. *Nat. Mater.* **2012**, *11*, 241–249.

[51] Yang, S. H.; Liu, Y. Y.; Hao, Y. F.; Yang, X. P.; Goddard III, W. A.; Zhang, X. L.; Cao, B. Q. Oxygen-vacancy abundant ultrafine Co_3O_4/graphene composites for high-rate supercapacitor electrodes. *Adv. Sci.* **2018**, *5*, 1700659.

[52] Pfleging, W. A review of laser electrode processing for development and manufacturing of lithium-ion batteries. *Nanophotonics* **2018**, *7*, 549–573.

[53] Orekhov, N. D.; Bondareva, J. V.; Potapov, D. O.; Dyakonov, P. V.; Dubinin, O. N.; Tarkhov, M. A.; Diudbin, G. D.; Maslakov, K. I.; Logunov, M. A.; Kvashnin, D. G. et al. Mechanism of graphene oxide laser reduction at ambient conditions: Experimental and ReaxFF study. *Carbon* **2022**, *191*, 546–554.

[54] Cui, H.; Song, Y. Z.; Ren, D. S.; Wang, L.; He, X. M. Electrocapillary boosting electrode wetting for high-energy lithium-ion batteries. *Joule* **2024**, *8*, 29–44.

[55] Awasthi, H.; Nishchitha, N. K.; Kumar, P. S.; Goel, S. Rapidly synthesized laser-induced graphene and its derivatives for miniaturized energy devices: Principles, applications, and challenges. *Appl. Phys. Rev.* **2025**, *12*, 021331.

[56] Pantrangi, M.; Ashalley, E.; Hadi, M. K.; Xiao, H.; Zhang, Y.; Ahmed, W.; Singh, N.; Alam, A.; Younis, U.; Ran, F. et al. Flexible micro-supercapacitors: Materials and architectures for smart integrated wearable and implantable devices. *Energy Storage Mater.* **2024**, *73*, 103791.

[57] Emelianov, A. V.; Pettersson, M.; Bobrinetskiy, I. I. Ultrafast laser processing of 2D materials: Novel routes to advanced devices. *Adv. Mater.* **2024**, *36*, 2402907.

[58] Xu, K. C.; Cai, Z. M.; Luo, H. Y.; Lu, Y. Y.; Ding, C. L.; Yang, G.; Wang, L. L.; Kuang, C. F.; Liu, J. Q.; Yang, H. Y. Toward integrated multifunctional laser-induced graphene-based skin-like flexible sensor systems. *ACS Nano* **2024**, *18*, 26435–26476.

[59] Ren, X. Y.; Mei, X. S.; Zhou, J. Z.; Wang, X. W.; Wei, F. Q.; Mei, H. H.; Zhao, S. J.; Lu, Y.; Cui, J. L. Laser-induced self-limiting welding of Ag nanowires with high mechanical and electrical performance. *Adv. Mater.* **2024**, *36*, 2408575.

[60] Fatkullin, M.; Cheshev, D.; Averkiev, A.; Gorbunova, A.; Murastov, G.; Liu, J. X.; Postnikov, P.; Cheng, C.; Rodriguez, R. D.; Sheremet, E. Photochemistry dominates over photothermal effects in the laser-induced reduction of graphene oxide by visible light. *Nat. Commun.* **2024**, *15*, 9711.

[61] Li, Z.; Song, J.; Hu, H. B.; Yuan, C. Z.; Wu, M. Z.; Ho, D. Rolled-up island-bridge (RIB): A new and general electrode configuration design for a wire-shaped stretchable micro-supercapacitor array. *J. Mater. Chem. A* **2021**, *9*, 2899–2911.

[62] Lee, J.; Lee, P.; Lee, H.; Lee, D.; Lee, S. S.; Ko, S. H. Very long Ag nanowire synthesis and its application in a highly transparent, conductive and flexible metal electrode touch panel. *Nanoscale* **2012**, *4*, 6408–6414.

[63] Yoon, H.; Choi, J.; Kim, J.; Kim, J.; Min, J.; Kim, D.; Jeong, S.; Lee, J. G.; Bang, J.; Choi, S. H. et al. Adaptive epidermal bioelectronics by highly breathable and stretchable metal nanowire bioelectrodes on electrospun nanofiber membrane. *Adv. Funct. Mater.* **2024**, *34*, 2313504.

[64] Wang, H. Z.; Jiao, X. Y.; Gao, Z. Q.; Hou, P. X.; Xu, L. L.; Shi, C.; Liang, Y.; Wang, Y. P.; Liu, C. Highly conductive double-wall carbon nanotube fibers produced by dry-jet wet spinning. *Adv. Funct. Mater.* **2024**, *34*, 2404538.

[65] Daneshvar, F.; Chen, H. X.; Zhang, T.; Sue, H. J. Fabrication of light-weight and highly conductive copper-carbon nanotube core-shell fibers through interface design. *Adv. Mater. Interfaces* **2020**, *7*, 2000779.

[66] De Silva, T.; Damery, C.; Alkhaldi, R.; Karunanithy, R.; Gallaba, D. H.; Patil, P. D.; Wasala, M.; Sivakumar, P.; Migone, A.; Talapatra, S. Carbon nanotube based robust and flexible solid-state supercapacitor. *ACS Appl. Mater. Interfaces* **2021**, *13*, 56004–56013.

[67] Gurova, O. A.; Sysoev, V. I.; Lobiak, E. V.; Makarova, A. A.; Asanov, I. P.; Okotrub, A. V.; Kulik, L. V.; Bulusheva, L. G. Enhancement of volumetric capacitance of binder-free single-walled carbon nanotube film via fluorination. *Nanomaterials* **2021**, *11*, 1135.

[68] Ramzan, H.; Nadeem, F.; Usman, M.; Shahzaib, M.; Ur Rahman, M.; Shen, F. H.; Zhang, Z. P.; Singhania, R. R.; Jabeen, F.; Afzal, W. et al. Investigating the quantum size effects of multi-walled carbon nanotubes (MWCNTs) in photocatalytic fermentative biohydrogen production. *J. Clean. Prod.* **2024**, *449*, 141738.

[69] Senokos, E.; Rana, M.; Vila, M.; Fernandez-Cestau, J.; Costa, R. D.; Marcilla, R.; Vilatela, J. J. Transparent and flexible high-power supercapacitors based on carbon nanotube fibre aerogels. *Nanoscale* **2020**, *12*, 16980–16986.

[70] Ke, Q. L.; Xu, Q. L.; Guo, C. C.; He, S. Y.; Zhang, J.; Zhang, Y. M.; Zhang, Y.; Zhang, K. Surface-functionalized carbon nanotube yarn for high-performing flexible supercapacitors. *ACS Appl. Energy Mater.* **2025**, *8*, 10813–10821.

[71] Murugan, N.; Thangarasu, S.; Venkatachalam, P.; Bhosale, M.; Kamalakannan, S.; Prakash, M.; Seo, S. B.; Choi, Y. R.; Kang, M.; Oh, T. H. et al. Holey carbon-nanotube-wrapped MXene for hydrogen evolution reactions and supercapacitor applications. *Int. J. Hydrogen Energy* **2023**, *48*, 38584–38601.

[72] Ahmad, K.; Oh, T. H. Recent progress in MXene-based materials for supercapacitors and electrochemical sensing applications. *Biosensors* **2025**, *15*, 288.

[73] Jung, Y.; Pyun, K. R.; Yu, S.; Ahn, J.; Kim, J.; Park, J. J.; Lee, M. J.; Lee, B.; Won, D.; Bang, J. et al. Laser-induced nanowire percolation interlocking for ultrarobust soft electronics. *Nano-Micro Lett.* **2025**, *17*, 127.

[74] De Chiara, B.; Del Duca, F.; Hussain, M. Z.; Kratky, T.; Banerjee, P.; Dummert, S. V.; Khoshouei, A.; Chanut, N.; Peng, H.; Al Boustani, G. et al. Laser-induced metal-organic framework-derived flexible electrodes for electrochemical sensing. *ACS Appl. Mater. Interfaces* **2025**, *17*, 3772–3784.

[75] Nguyen, P. T.; Jang, J.; Lee, Y.; Choi, S. T.; In, J. B. Laser-assisted fabrication of flexible monofilament fiber supercapacitors. *J. Mater. Chem. A* **2021**, *9*, 4841–4850.

[76] Yang, C.; Trikantzopoulos, E.; Nguyen, M. D.; Jacobs, C. B.; Wang, Y.; Mahjouri-Samani, M.; Ivanov, I. N.; Venton, B. J. Laser treated carbon nanotube yarn microelectrodes for rapid and sensitive detection of dopamine *in vivo*. *ACS Sens.* **2016**, *1*, 508–515.

[77] Yu, Y. C.; Deng, Y. B.; Hasan, M. A. A.; Bai, Y. F.; Li, R. Z.; Deng, S. G.; Joshi, P.; Shin, S.; Hu, A. M. Femtosecond laser-induced non-thermal welding for a single Cu nanowire glucose sensor. *Nanoscale Adv.* **2020**, *2*, 1195–1205.

[78] Velasco, A.; Ryu, Y. K.; Hamada, A.; de Andrés, A.; Calle, F.; Martinez, J. Laser-induced graphene microsupercapacitors: Structure, quality, and performance. *Nanomaterials* **2023**, *13*, 788.

[79] Zhou, T. Z.; Wu, C.; Wang, Y. L.; Tomsia, A. P.; Li, M. Z.; Saiz, E.; Fang, S. L.; Baughman, R. H.; Jiang, L.; Cheng, Q. F. Super-tough MXene-functionalized graphene sheets. *Nat. Commun.* **2020**, *11*, 2077.

[80] Alem, A. F.; Worku, A. K.; Ayele, D. W.; Wubieneh, T. A.; Teshager, A. A.; Kndie, T. M.; Admasu, B. T.; Teshager, M. A.; Asege, A. A.; Ambaw, M. D. et al. Ag doped Co_3O_4 nanoparticles for high-performance supercapacitor application. *Heliyon* **2023**, *9*, e13286.

[81] Worku, A. K.; Ayele, D. W. Recent advances of graphene-based materials for emerging technologies. *Results Chem.* **2023**, *5*, 100971.

[82] Tiliakos, A.; Ceaus, C.; Iordache, S. M.; Vasile, E.; Stamatin, I. Morphic transitions of nanocarbons via laser pyrolysis of polyimide films. *J. Anal. Appl. Pyrolysis* **2016**, *121*, 275–286.

[83] Wang, F. C.; Wang, K. D.; Zheng, B. X.; Dong, X.; Mei, X. S.; Lv, J.; Duan, W. Q.; Wang, W. J. Laser-induced graphene: Preparation, functionalization and applications. *Mater. Technol.* **2018**, *33*, 340–356.

[84] Ladrón-de-Guevara, A.; Boscá, A.; Pedrós, J.; Climent-Pascual, E.; de Andrés, A.; Calle, F.; Martínez, J. Reduced graphene oxide/polyaniline electrochemical supercapacitors fabricated by laser. *Appl. Surf. Sci*. **2019**, *467–468*, 691–697.

[85] Clerici, F.; Fontana, M.; Bianco, S.; Serrapede, M.; Perrucci, F.; Ferrero, S.; Tresso, E.; Lamberti, A. *In situ* MoS_2 decoration of laser-induced graphene as flexible supercapacitor electrodes. *ACS Appl. Mater. Interfaces* **2016**, *8*, 10459–10465.

[86] Cao, L. J.; Zhu, S. R.; Pan, B. H.; Dai, X. Y.; Zhao, W. W.; Liu, Y.; Xie, W. P.; Kuang, Y. B.; Liu, X. Q. Stable and durable laser-induced graphene patterns embedded in polymer substrates. *Carbon* **2020**, *163*, 85–94.

[87] Avinash, K.; Patolsky, F. Laser-induced graphene structures: From synthesis and applications to future prospects. *Mater. Today* **2023**, *70*, 104–136.

[88] Le, T. S. D.; Phan, H. P.; Kwon, S.; Park, S.; Jung, Y.; Min, J.; Chun, B. J.; Yoon, H.; Ko, S. H.; Kim, S. W. et al. Recent advances in laser-induced graphene: Mechanism, fabrication, properties, and applications in flexible electronics. *Adv. Funct. Mater.* **2022**, *32*, 2205158.

[89] Shahzad, F.; Iqbal, A.; Kim, H.; Koo, C. M. 2D transition metal carbides (MXenes): Applications as an electrically conducting material. *Adv. Mater.* **2020**, *32*, 2002159.

[90] Ying, G. B.; Kota, S.; Dillon, A. D.; Fafarman, A. T.; Barsoum, M. W. Conductive transparent V_2CT_x (MXene) films. *FlatChem* **2018**, *8*, 25–30.

[91] Liu, L. Y.; Zschiesche, H.; Antonietti, M.; Daffos, B.; Tarakina, N. V.; Gibilaro, M.; Chamelot, P.; Massot, L.; Duployer, B.; Taberna, P. L. et al. Tuning the surface chemistry of MXene to improve energy storage: Example of nitrification by salt melt. *Adv. Energy Mater.* **2023**, *13*, 2202709.

[92] Yao, Y. Y.; Zhang, X. H.; Tan, L.; Pan, J.; Zhan, C. W.; Liu, W. F.; Feng, Y. M.; Li, H. X.; Xiong, L. $Ti_3C_2T_x$ nanosheet-based electrode with high capacitance enabled by nitrogen doping and surface modification. *ACS Appl. Nano Mater.* **2024**, *7*, 15143–15152.

[93] Yip, B. R. P.; Chen, C. F.; Jiang, Y.; Ohayon, D.; Bazan, G. C.; Wang, X. H. Aqueous asymmetric pseudocapacitor featuring high areal energy and power using conjugated polyelectrolytes and $Ti_3C_2T_x$ MXene. *Nat. Commun.* **2025**, *16*, 7984.

[94] Depijan, M.; Hantanasirisakul, K.; Pakawatpanurut, P. Interfacial engineering of $Ti_3C_2T_x$ MXene electrode using g-C_3N_4 nanosheets for high-performance supercapacitor in neutral electrolyte. *ACS Omega* **2024**, *9*, 22256–22264.

[95] Mateen, A.; Ahmad, Z.; Ali, S.; Hassan, N. U.; Ahmed, F.; Alshgari, R. A.; Mushab, M.; Eldin, S. M.; Ansari, M. Z.; Javed, M. S. et al. Silicon intercalation on MXene nanosheets towards new insights into a superior electrode material for high-performance Zn-ion supercapacitor. *J. Energy Storage* **2023**, *71*, 108151.

[96] Mu, J. P.; Zhao, Y. X.; Guo, Z. C.; Zhang, Z. X.; Che, H. W.; Wang, Y. M.; Zhang, X. L.; Wang, G. S.; Mu, J. B.; Wang, L. Rational design of new, efficient, and suitable nickel phthalocyanine reinforced MXene electrodes for supercapacitors. *J. Energy Storage* **2023**, *61*, 106768.

[97] Wang, Y. B.; Chen, N. J.; Zhou, B.; Zhou, X. F.; Pu, B.; Bai, J.; Tang, Q.; Liu, Y.; Yang, W. Q. NH_3-induced *in situ* etching strategy derived 3D-interconnected porous MXene/carbon dots films for high performance flexible supercapacitors. *Nano-Micro Lett.* **2023**, *15*, 231.

[98] Ghosh, K.; Ghosh, J.; Giri, P. K. Accordion-like multilayered two-dimensional $Ti_3C_2T_x$ MXenes for catalytic elimination of organic dyes from wastewater via the Fenton reaction. *ACS Appl. Nano Mater.* **2022**, *5*, 16451–16461.

[99] Wang, G. X.; Zhang, R.; Zhang, H. Q.; Cheng, K. Aqueous MXene inks for inkjet-printing microsupercapacitors with ultrahigh energy densities. *J. Colloid Interface Sci.* **2023**, *645*, 359–370.

[100] Huang, H. C.; Yang, W. Q. MXene-based micro-supercapacitors: Ink rheology, microelectrode design and integrated system. *ACS Nano* **2024**, *18*, 4651–4682.

[101] Yuan, M. M.; Wang, L. B.; Liu, X. Q.; Du, X. Y.; Zhang, G. B.; Chang, Y. K.; Xia, Q. X.; Hu, Q. K.; Zhou, A. G. 3D printing quasi-solid-state micro-supercapacitors with ultrahigh areal energy density based on high concentration MXene sediment. *Chem. Eng. J.* **2023**, *451*, 138686.

[102] Qin, J. Q.; Das, P.; Zheng, S. H.; Wu, Z. S. A perspective on two-dimensional materials for planar micro-supercapacitors. *APL Mater.* **2019**, *7*, 090902.

[103] Verger, L.; Xu, C.; Natu, V.; Cheng, H. M.; Ren, W. C.; Barsoum, M. W. Overview of the synthesis of MXenes and other ultrathin 2D transition metal carbides and nitrides. *Curr. Opin. Solid State Mater. Sci.* **2019**, *23*, 149–163.

[104] Wang, M.; Feng, S.; Bai, C.; Ji, K.; Zhang, J.; Wang, S.; Lu, Y.; Kong, D. Ultrastretchable MXene Microsupercapacitors. *Small* **2023**, *19*, 2300386.

[105] Chen, X.; Wang, S. L.; Shi, J. J.; Du, X. Y.; Cheng, Q. H.; Xue, R.; Wang, Q.; Wang, M.; Ruan, L. M.; Zeng, W. Direct laser etching free-standing MXene-MoS_2 film for highly flexible micro-supercapacitor. *Adv. Mater. Interfaces* **2019**, *6*, 1901160.

[106] Li, Q.; Wang, Q. Z.; Li, L. L.; Yang, L. J.; Wang, Y.; Wang, X. H.; Fang, H. T. Femtosecond laser-etched MXene microsupercapacitors with double-side configuration via arbitrary on- and through-substrate connections. *Adv. Energy Mater.* **2020**, *10*, 2000470.

[107] Hondred, J. A.; Stromberg, L. R.; Mosher, C. L.; Claussen, J. C. High-resolution graphene films for electrochemical sensing via inkjet maskless lithography. *ACS Nano* **2017**, *11*, 9836–9845.

[108] Ye, J. L.; Tan, H. B.; Wu, S. L.; Ni, K.; Pan, F.; Liu, J.; Tao, Z. C.; Qu, Y.; Ji, H. X.; Simon, P. et al. Direct laser writing of graphene made from chemical vapor deposition for flexible, integratable micro-supercapacitors with ultrahigh power output. *Adv. Mater.* **2018**, *30*, 1801384.

[109] Choi, H.; Nguyen, P. T.; In, J. B. Laser transmission welding and surface modification of graphene film for flexible supercapacitor applications. *Appl. Surf. Sci.* **2019**, *483*, 481–488.

[110] Gao, J.; Shao, C. X.; Shao, S. X.; Bai, C. C.; Khalil, U. R.; Zhao, Y.; Jiang, L.; Qu, L. T. Laser-assisted multiscale fabrication of configuration-editable supercapacitors with high energy density. *ACS Nano* **2019**, *13*, 7463–7470.

[111] Shi, H. H.; Jang, S.; Naguib, H. E. Freestanding laser-assisted reduced graphene oxide microribbon textile electrode fabricated on a liquid surface for supercapacitors and breath sensors. *ACS Appl. Mater. Interfaces* **2019**, *11*, 27183–27191.

[112] Wang, H.; Wu, Y.; Ma, M. Y.; Dong, S.; Li, Q.; Du, J.; Zhang, H.; Xu, Q. Y. Pulsed laser deposition of $CsPbBr_3$ films for application in perovskite solar cells. *ACS Appl. Energy Mater.* **2019**, *2*, 2305–2312.

[113] Lee, J.; Seok, J. Y.; Son, S.; Yang, M. Y.; Kang, B. High-energy,

flexible micro-supercapacitors by one-step laser fabrication of a self-generated nanoporous metal/oxide electrode. *J. Mater. Chem. A* **2017**, *5*, 24585–24593.

[114] Henning, R. A.; Uredat, P.; Simon, C.; Bloesser, A.; Cop, P.; Elm, M. T.; Marschall, R. Characterization of MFe_2O_4 (M = Mg, Zn) thin films prepared by pulsed laser deposition for photoelectrochemical applications. *J. Phys. Chem. C* **2019**, *123*, 18240–18247.

[115] Pan, R. J.; Rau, D.; Moryson, Y.; Sann, J.; Janek, J. Reversible capacity loss of $LiCoO_2$ thin film electrodes. *ACS Appl. Energy Mater.* **2020**, *3*, 6065–6071.

[116] Lethien, C.; Le Bideau, J.; Brousse, T. Challenges and prospects of 3D micro-supercapacitors for powering the internet of things. *Energy Environ. Sci.* **2019**, *12*, 96–115.

[117] Liu, H. Z.; Zhang, G. H.; Wang, L.; Zhang, X. N.; Zhao, Z. X.; Chen, F. J.; Song, L. J.; Duan, H. G. Engineering 3D architecture electrodes for high-rate aqueous Zn–Mn microbatteries. *ACS Appl. Energy Mater.* **2021**, *4*, 10414–10422.

[118] Gillis, W. F.; Lissandrello, C. A.; Shen, J.; Pearre, B. W.; Mertiri, A.; Deku, F.; Cogan, S.; Holinski, B. J.; Chew, D. J.; White, A. E. et al. Carbon fiber on polyimide ultra-microelectrodes. *J. Neural Eng.* **2018**, *15*, 016010.

[119] Zhang, C.; Peng, Z. X.; Huang, C. L.; Zhang, B. W.; Xing, C.; Chen, H. M.; Cheng, H. Y.; Wang, J.; Tang, S. L. High-energy all-in-one stretchable micro-supercapacitor arrays based on 3D laser-induced graphene foams decorated with mesoporous ZnP nanosheets for self-powered stretchable systems. *Nano Energy* **2021**, *81*, 105609.

[120] Lee, C. Y.; Taylor, A. C.; Beirne, S.; Wallace, G. G. 3D-printed conical arrays of TiO_2 electrodes for enhanced photoelectrochemical water splitting. *Adv. Energy Mater.* **2017**, *7*, 1701060.

[121] Kundu, A.; McCoy, L.; Azim, N.; Nguyen, H.; Didier, C. M.; Ausaf, T.; Sharma, A. D.; Curley, J. L.; Moore, M. J.; Rajaraman, S. Fabrication and characterization of 3D printed, 3D microelectrode arrays for interfacing with a peripheral nerve-on-a-chip. *ACS Biomater. Sci. Eng.* **2021**, *7*, 3018–3029.

[122] Soscia, D. A.; Lam, D.; Tooker, A. C.; Enright, H. A.; Triplett, M.; Karande, P.; Peters, S. K. G.; Sales, A. P.; Wheeler, E. K.; Fischer, N. O. A flexible 3-dimensional microelectrode array for in vitro brain models. *Lab Chip* **2020**, *20*, 901–911.

[123] Chen, C. Z.; Ran, B.; Wang, Z. X.; Zhao, H. L.; Lan, M. B.; Chen, H. Y.; Zhu, Y. G. Development of micropillar array electrodes for highly sensitive detection of biomarkers. *RSC Adv.* **2020**, *10*, 41110–41119.

[124] Kim, C.; Kang, D. Y.; Moon, J. H. Full lithographic fabrication of boron-doped 3D porous carbon patterns for high volumetric energy density microsupercapacitors. *Nano Energy* **2018**, *53*, 182–188.

[125] Li, C. M.; Li, X. M.; Yang, Q. Z.; Sun, P. C.; Wu, L. F.; Nie, B. B.; Tian, H. M.; Wang, Y. C.; Wang, C. H.; Chen, X. L. et al. Tuning the mechanical and electrical properties of porous electrodes for architecting 3D microsupercapacitors with batteries-level energy. *Adv. Sci.* **2021**, *8*, 2004957.

[126] Cho, G. B.; Kim, J. K.; Lee, S. H.; Kim, G. T.; Noh, J. P.; Cho, K. K.; Kim, K. W.; Nam, T. H.; Ahn, H. J. Facile fabrication of patterned Si film electrodes containing trench-structured Cu current collectors for thin-film batteries. *Electrochim. Acta* **2017**, *224*, 649–659.

[127] Zhu, P. C.; Boyce, A.; Daemi, S. R.; Dong, B.; Chen, Y. X.; Guan, S. L.; Crozier, M.; Chiu, Y. L.; Davenport, A. J.; Jervis, R. et al. A groovy laser processing route to achieving high power and energy lithium-ion batteries. *Energy Storage Mater.* **2024**, *69*, 103373.

[128] Manshina, A. A.; Tumkin, I. I.; Khairullina, E. M.; Mizoshiri, M.; Ostendorf, A.; Kulinich, S. A.; Makarov, S.; Kuchmizhak, A. A.; Gurevich, E. L. The second laser revolution in chemistry: Emerging laser technologies for precise fabrication of multifunctional nanomaterials and nanostructures. *Adv. Funct. Mater.* **2024**, *34*, 2405457.

[129] Jia, Y. H.; Gong, X.; Peng, P.; Wang, Z. D.; Tian, Z. Z.; Ren, L. M.; Fu, Y. Y.; Zhang, H. Toward high carrier mobility and low contact resistance: Laser cleaning of PMMA residues on graphene surfaces. *Nano-Micro Lett.* **2016**, *8*, 336–346.

[130] Do, H. M.; Ryu, C.; In, J. B. Laser additive-subtractive microfabrication of three-dimensional microsupercapacitor electrodes. *Chem. Eng. J.* **2025**, *514*, 163400.

[131] Xu, G. Y.; Jarjes, Z. A.; Desprez, V.; Kilmartin, P. A.; Travas-Sejdic, J. Sensitive, selective, disposable electrochemical dopamine sensor based on PEDOT-modified laser scribed graphene. *Biosens. Bioelectron.* **2018**, *107*, 184–191.

[132] Zhao, Y. F.; Luo, M.; Hu, Y. J.; Cheng, H. H.; Yan, J. F.; Jiang, L.; Qu, L. T. Laser micro/Nano fabrication of electrochemical filtering capacitors: Multiscale structural engineering for high-frequency power conditioning. *Adv. Energy Mater.* **2025**, *15*, e02620.

[133] Kyerematen, N. A.; Brousse, T.; Pech, D. Microsupercapacitors as miniaturized energy-storage components for on-chip electronics. *Nat. Nanotechnol.* **2017**, *12*, 7–15.

[134] Velasco, A.; Ryu, Y. K.; Boscá, A.; Ladrón-de-Guevara, A.; Hunt, E.; Zuo, J. H.; Pedrós, J.; Calle, F.; Martinez, J. Recent trends in graphene supercapacitors: From large area to microsupercapacitors. *Sustainable Energy Fuels* **2021**, *5*, 1235–1254.

[135] Li, X. Y.; Jin, X. T.; Wang, Y.; Zhang, X. Q.; Li, D.; Wang, J. Q.; Yuan, M.; Liu, J. J.; Zhao, Y. All-direct laser patterning zinc-based microbatteries. *Adv. Funct. Mater.* **2024**, *34*, 2314060.

[136] Jin, X. T.; Song, L.; Dai, C. L.; Xiao, Y. K.; Han, Y. Y.; Li, X. Y.; Wang, Y.; Zhang, J. T.; Zhao, Y.; Zhang, Z. P. et al. A flexible aqueous zinc-iodine microbattery with unprecedented energy density. *Adv. Mater.* **2022**, *34*, 2109450.

[137] Dai, C. L.; Hu, L. Y.; Jin, X. T.; Wang, Y.; Wang, R.; Xiao, Y. K.; Li, X. Y.; Zhang, X. Q.; Song, L.; Han, Y. Y. et al. Fast constructing polarity-switchable zinc-bromine microbatteries with high areal energy density. *Sci. Adv.* **2022**, *8*, eabo6688.

[138] Jung, J.; Jeong, J. R.; Lee, J.; Lee, S. H.; Kim, S. Y.; Kim, M. J.; Nah, J.; Lee, M. H. *In situ* formation of graphene/metal oxide composites for high-energy microsupercapacitors. *NPG Asia Mater.* **2020**, *12*, 50.

[139] Wang, Y.; Hong, X. F.; Guo, Y. Q.; Zhao, Y. L.; Liao, X. B.; Liu, X.; Li, Q.; He, L.; Mai, L. Q. Wearable textile-based Co−Zn alkaline microbattery with high energy density and excellent reliability. *Small* **2020**, *16*, 2000293.

[140] Lee, S. H.; Lee, J.; Jung, J.; Cho, A. R.; Jeong, J. R.; Van, C. D.; Nah, J.; Lee, M. H. Enhanced electrochemical performance of micro-supercapacitors via laser-scribed cobalt/reduced graphene oxide hybrids. *ACS Appl. Mater. Interfaces* **2021**, *13*, 18821–18828.

[141] Jiang, Z. M.; Sheng, L. Z.; Lin, Y. Q.; Zhang, S.; Zhang, L. H.; Wei, T.; Zhou, J. L.; Liu, C. Q.; Jiang, H.; Zhou, Q. H. et al. Weldable and flexible graphene ribbon@Ni fibers with ultrahigh length capacitance for all-solid-state supercapacitors. *Chem. Eng. J.* **2021**, *426*, 131361.

[142] Lei, Y. J.; Zhao, W. L.; Zhu, Y. P.; Buttner, U.; Dong, X. C.; Alshareef, H. N. Three-dimensional $Ti_3C_2T_x$ MXene-Prussian blue hybrid microsupercapacitors by water lift-off lithography. *ACS Nano* **2022**, *16*, 1974–1985.

[143] Xue, H.; Huang, P. H.; Lai, L. L.; Su, Y. C.; Strömberg, A.; Cao, G. L.; Fan, Y. Z.; Khartsev, S.; Göthelid, M.; Sun, Y. T. et al. High-rate metal-free MXene microsupercapacitors on paper substrates. *Carbon Energy* **2024**, *6*, e442.

[144] Yuan, Y. J.; Li, X.; Jiang, L.; Liang, M. S.; Zhang, X. Q.; Wu, S. Y.; Wu, J. R.; Tian, M. Y.; Zhao, Y.; Qu, L. T. Laser maskless fast patterning for multitype microsupercapacitors. *Nat. Commun.* **2023**, *14*, 3967.

[145] Yuan, Y. J.; Jiang, L.; Li, X.; Zuo, P.; Xu, C. Y.; Tian, M. Y.; Zhang, X. Q.; Wang, S. M.; Lu, B.; Shao, C. X. et al. Laser photonic-reduction stamping for graphene-based micro-supercapacitors ultrafast fabrication. *Nat. Commun.* **2020**, *11*, 6185.

[146] Pazhamalai, P.; Krishnamoorthy, K.; Sahoo, S.; Mariappan, V. K.; Kim, S. J. Copper tungsten sulfide anchored on Ni-foam as a high-performance binder free negative electrode for asymmetric supercapacitor. *Chem. Eng. J.* **2019**, *359*, 409–418.

[147] Shen, D. Z.; Zou, G. S.; Liu, L.; Zhao, W. Z.; Wu, A. P.; Duley, W. W.; Zhou, Y. N. Scalable high-performance ultraminiature graphene micro-supercapacitors by a hybrid technique combining direct writing and controllable microdroplet transfer. *ACS Appl. Mater. Interfaces* **2018**, *10*, 5404–5412.

[148] Kamboj, N.; Purkait, T.; Das, M.; Sarkar, S.; Hazra, K. S.; Dey, R. S. Ultralong cycle life and outstanding capacitive performance of a 10.8 V metal free micro-supercapacitor with highly conducting and robust laser-irradiated graphene for an integrated storage device. *Energy Environ. Sci.* **2019**, *12*, 2507–2517.

[149] Xu, R. Q.; Liu, P.; Ji, G. H.; Gao, L. J.; Zhao, J. Versatile strategy to design flexible planar-integrated microsupercapacitors based on Co_3O_4-decorated laser-induced graphene. *ACS Appl. Energy Mater.* **2020**, *3*, 10676–10684.

[150] Liu, H. L.; Gan, L. T.; Chen, R. J.; Xiao, Z. W.; Chen, Y.; Yang, H. Z.; Liu, Y. H.; Wu, B. S.; Wong, C. P.; Chen, X. 3D graphene paper-based tandem metal-free thin-film supercapacitors with integrated 200 V output. *Int. J. Extrem. Manuf.* **2025**, *7*, 055501.

[151] Sha, Y.; Zhu, M. H.; Huang, K.; Zhang, Y.; Moissinac, F.; Zhang, Z. Z.; Cheng, D. X.; Mativenga, P.; Liu, Z. Towards a new avenue for rapid synthesis of electrocatalytic electrodes via laser-induced hydrothermal reaction for water splitting. *Int. J. Extrem. Manuf.* **2024**, *6*, 015502.

[152] Kim, S. J.; Lee, H. E.; Choi, H.; Kim, Y.; We, J. H.; Shin, J. S.; Lee, K. J.; Cho, B. J. High-performance flexible thermoelectric power generator using laser multiscanning lift-off process. *ACS Nano* **2016**, *10*, 10851–10857.

[153] Yan, Y. G.; Geng, W. Q.; Qiu, J. H.; Ke, H. Q.; Luo, C.; Yang, J. H.; Uher, C.; Tang, X. F. Thermoelectric properties of n-type ZrNiSn prepared by rapid non-equilibrium laser processing. *RSC Adv.* **2018**, *8*, 15796–15803.

[154] Wu, H.; Ye, F.; Yang, M.; Luo, F.; Tang, X. Y.; Tang, Q.; Qiu, H. R.; Huang, Z. P.; Wang, G. S.; Sun, Z. Q. et al. Silicon heterojunction back-contact solar cells by laser patterning. *Nature* **2024**, *635*, 604–609.

[155] Yi, J. P.; Bailey, C.; Leung, T. L.; Tao, R. M.; Wang, G. L.; Bing, J. M.; Mahmud, M. A.; Mckenzie, D. R.; Ho-Baillie, A. W. Y. Efficient ambient-all-laser-annealed wide bandgap perovskite solar cells. *Adv. Funct. Mater.* **2025**, *35*, 2503971.

[156] Meng, J. Q.; Chen, X. Y.; Li, W. H.; Chai, N. Y.; Zeng, Z. L.; Yue, Y. F.; Zhao, F. Y.; Wang, X. W. Ultrafast laser irradiation induced oxidation of dopant-free Spiro-OMeTAD for improving the perovskite solar cells performance. *Energy Environ. Mater.* **2025**, *8*, e12818.

[157] Wu, K. P.; Yan, Y. G.; Zhang, J.; Mao, Y.; Xie, H. Y.; Yang, J. H.; Zhang, Q. J.; Uher, C.; Tang, X. F. Preparation of n-type Bi_2Te_3 thermoelectric materials by non-contact dispenser printing combined with selective laser melting. *Phys. Status Solidi Rapid Res. Lett.* **2017**, *11*, 1700067.

[158] Zhang, J.; Zhang, T.; Zhang, H.; Wang, Z.; Li, C.; Wang, Z. X.; Li, K. W.; Huang, X. M.; Chen, M.; Chen, Z. et al. Single-crystal SnSe thermoelectric fibers via laser-induced directional crystallization: From 1D fibers to multidimensional fabrics. *Adv. Mater.* **2020**, *32*, 2002702.

[159] Chen, T. H.; Chen, P. H.; Chen, C. H. Laser co-ablation of bismuth antimony telluride and diamond-like carbon nanocomposites for enhanced thermoelectric performance. *J. Mater. Chem. A* **2018**, *6*, 982–990.

[160] Chen, S. C.; She, N. Z.; Wu, K. H.; Chen, Y. Z.; Lin, W. S.; Li, J. X.; Lai, F. I.; Juang, J. Y.; Luo, C. W.; Cheng, L. T. et al. Crystalline engineering toward large-scale high-efficiency printable $Cu(In,Ga)Se_2$ thin film solar cells on flexible substrate by femtosecond laser annealing process. *ACS Appl. Mater. Interfaces* **2017**, *9*, 14006–14012.

[161] Wilkes, G. C.; Deng, X. Y.; Choi, J. J.; Gupta, M. C. Laser annealing of TiO_2 electron-transporting layer in perovskite solar cells. *ACS Appl. Mater. Interfaces* **2018**, *10*, 41312–41317.

[162] Tai, M. Q.; Zhao, X. Y.; Wei, H. M.; Wang, G.; Hao, F.; Li, X.; Yin, X. W.; Zhou, Y.; Han, J. H.; Wei, Y. et al. Laser-induced flash-evaporation printing $CH_3NH_3PbI_3$ thin films for high-performance planar solar cells. *ACS Appl. Mater. Interfaces* **2018**, *10*, 26206–26212.

[163] Hadi, A.; Chen, Q.; Curioni, M.; Xiao, R. S.; Huang, T.; Liu, Z. One-step fiber laser fabrication of mesoporous and compact TiO_2 layers for enhanced performance of dye-sensitized solar cells. *ACS Sustainable Chem. Eng.* **2018**, *6*, 12299–12308.

[164] Belchi, R.; Habert, A.; Foy, E.; Gheno, A.; Vedraine, S.; Antony, R.; Ratier, B.; Bouclé, J.; Herlin-Boime, N. One-step synthesis of TiO_2/graphene nanocomposites by laser pyrolysis with well-controlled properties and application in perovskite solar cells. *ACS Omega* **2019**, *4*, 11906–11913.

[165] Cao, Q.; Shin, M.; Lavrik, N. V.; Venton, B. J. 3D-printed carbon nanoelectrodes for *in vivo* neurotransmitter sensing. *Nano Lett.* **2020**, *20*, 6831–6836.

[166] Yang, Y. R.; Song, Y.; Bo, X. J.; Min, J. H.; Pak, O. S.; Zhu, L. L.; Wang, M. Q.; Tu, J. B.; Kogan, A.; Zhang, H. X. et al. A laser-engraved wearable sensor for sensitive detection of uric acid and tyrosine in sweat. *Nat. Biotechnol.* **2020**, *38*, 217–224.

[167] Meng, L. Y.; Turner, A. P. F.; Mak, W. C. Conducting polymer-reinforced laser-irradiated graphene as a heterostructured 3D transducer for flexible skin patch biosensors. *ACS Appl. Mater. Interfaces* **2021**, *13*, 54456–54465.

[168] Lei, Y. J.; Alshareef, A. H.; Zhao, W. L.; Inal, S. Laser-scribed graphene electrodes derived from lignin for biochemical sensing. *ACS Appl. Nano Mater.* **2020**, *3*, 1166–1174.

[169] Gao, X. H.; Feng, W. S.; Zhu, Z.; Wu, Z. P.; Li, S.; Kan, S. T.; Qiu, X. Q.; Guo, A. M.; Chen, W.; Yin, K. Rapid fabrication of superhydrophilic micro/nanostructured nickel foam toward high-performance glucose sensor. *Adv. Mater. Interfaces* **2021**, *8*, 2002133.

[170] Cheng, C.; Wang, S. T.; Wu, J.; Yu, Y. C.; Li, R. Z.; Eda, S.; Chen, J. G.; Feng, G. Y.; Lawrie, B.; Hu, A. M. Bisphenol a sensors on polyimide fabricated by laser direct writing for onsite river water monitoring at Attomolar concentration. *ACS Appl. Mater. Interfaces* **2016**, *8*, 17784–17792.

[171] Song, M. M.; Dang, L. T.; Long, J.; Hu, C. G. Laser-cut polymer tape templates for scalable filtration fabrication of user-designed and carbon-nanomaterial-based electrochemical sensors. *ACS Sens.* **2018**, *3*, 2518–2525.

[172] Lonsdale, W.; Wajrak, M.; Alameh, K. Manufacture and application of RuO_2 solid-state metal-oxide pH sensor to common beverages. *Talanta* **2018**, *180*, 277–281.

[173] Yan, W. H.; Yan, W. R.; Chen, T. D.; Xu, J. G.; Tian, Q.; Ho, D. Size-tunable flowerlike MoS_2 nanospheres combined with laser-induced graphene electrodes for NO_2 sensing. *ACS Appl. Nano Mater.* **2020**, *3*, 2545–2553.

[174] Beduk, T.; Beduk, D.; de Oliveira Filho, J. I.; Zihnioglu, F.; Cicek, C.; Sertoz, R.; Arda, B.; Goksel, T.; Turhan, K.; Salama, K. N. et al. Rapid point-of-care COVID-19 diagnosis with a gold-nanoarchitecture-assisted laser-scribed graphene biosensor. *Anal. Chem.* **2021**, *93*, 8585–8594.

[175] Yu, Y. C.; Joshi, P. C.; Wu, J.; Hu, A. M. Laser-induced carbon-

based smart flexible sensor array for multiflavors detection. *ACS Appl. Mater. Interfaces* **2018**, *10*, 34005–34012.

[176] Lim, H.; Kwon, H.; Kang, H.; Jang, J. E.; Kwon, H. J. Semiconducting MOFs on ultraviolet laser-induced graphene with a hierarchical pore architecture for NO_2 monitoring. *Nat. Commun.* **2023**, *14*, 3114.

[177] Harris, K. D.; Elias, A. L.; Chung, H. J. Flexible electronics under strain: A review of mechanical characterization and durability enhancement strategies. *J. Mater. Sci.* **2016**, *51*, 2771–2805.

[178] Riley, S.; Shevchuk, A.; George, C. Achieving dynamic stability and electromechanical resilience for ultra-flexible battery technology. *Commun. Mater.* **2024**, *5*, 268.

[179] Zardetto, V.; Brown, T. M.; Reale, A.; Di Carlo, A. Substrates for flexible electronics: A practical investigation on the electrical, film flexibility, optical, temperature, and solvent resistance properties. *J. Polym. Sci. B: Polym. Phys.* **2011**, *49*, 638–648.

[180] Lee, B.; Cho, H.; Jeong, S.; Yoon, J.; Jang, D.; Lee, D. K.; Kim, D.; Chung, S.; Hong, Y. Stretchable hybrid electronics: Combining rigid electronic devices with stretchable interconnects into high-performance on-skin electronics. *J. Inf. Disp.* **2022**, *23*, 163–184.

[181] Keum, K.; Yang, S.; Kim, K. S.; Park, S. K.; Kim, Y. H. Recent progress of stretchable displays: A comprehensive review of materials, device architectures, and applications. *Soft Sci.* **2024**, *4*, 34.

[182] Lee, J.; Liu, J. Flexible and stretchable bioelectronics for organoids. *Med-X* **2025**, *3*, 5.

[183] Zhang, G. J.; Gao, Z. J.; Zhu, C. Y.; Cui, F. H.; Jiang, Z. J.; Pan, R.; Shen, J. X.; Zhu, L.; Jiang, B. W.; Sun, L. T. et al. Multifunctional flexible self-supporting film electrode for wearable energy-storage sensing system. *Chem. Eng. J.* **2024**, *502*, 157929.

[184] Wang, L. N.; Tang, Y. X.; Li, Y.; Liu, C. Y.; Wei, N.; Zeng, W.; Liang, D. W. Multifunctional integrated interdigital microsupercapacitors and self-powered iontronic tactile pressure sensor for wearable electronics. *ACS Appl. Mater. Interfaces* **2022**, *14*, 47136–47147.

[185] Wang, T.; Pan, R. T.; Martins, M. L.; Cui, J. L.; Huang, Z. N.; Thapaliya, B. P.; Do-Thanh, C. L.; Zhou, M. S.; Fan, J. T.; Yang, Z. Z. et al. Machine-learning-assisted material discovery of oxygen-rich highly porous carbon active materials for aqueous supercapacitors. *Nat. Commun.* **2023**, *14*, 4607.

[186] Liu, J. B.; Jiang, F.; Tashiro, S.; Chen, S. J.; Tanaka, M. A physics-informed and data-driven framework for robotic welding in manufacturing. *Nat. Commun.* **2025**, *16*, 4807.